Aus dem Institut für Biomaterialforschung Helmholtz-Zentrum Geesthacht

Elasticity of fiber meshes derived from multiblock copolymers influences cell behaviors

Dissertation

zur Erlangung des akademischen Grades

"doctor rerum naturalium "

(Dr. rer. nat.)

in der Wissenschaftsdisziplin „Materialien in den Lebenswissenschaften"

eingereicht an der

Mathematisch-Naturwissenschaftlichen Fakultät

Institut für Biowissenschaften

der Universität Potsdam

von

Xianlei Sun

Aus Shandong, China

Potsdam, January 2022

Declaration

I, Xianlei Sun, formally submit this dissertation entitled, 'Elasticity of fiber meshes derived from multiblock copolymers influences cell behaviors', to the Institute of Biochemistry and Biology, Faculty of Science of the Universität Potsdam, Germany, for the academic degree of Doctor of Nature Sciences (Dr. rer. nat.) in the topic of 'Materials in Life Sciences'.

I hereby declare that this submission is totally original work of mine, performed between October 2015 to October 2019, and that, to my best knowledge and belief, no data has been included that was published online or released by another individual, unless where a proper citation is made within this thesis. Any parts of this dissertation have not been submitted to any other University or academic Institution for any other degree and qualification before. Any contributions to this study provided by those with whom I have collaborated at 'Helmholtz-Zentrum Geesthacht, Institute of Biomaterial Science' or elsewhere, are mentioned directly in the thesis.

<div align="right">

Xianlei Sun

Potsdam, May 2021

</div>

Acknowledgements

Contents

Contents

Abstract

Objective: The behaviors of endothelial cells or mesenchymal stem cells are remarkably influenced by the mechanical properties of their surrounding microenvironments. Here, electrospun fiber meshes containing various mechanical characteristics were developed from polyetheresterurethane (PEEU) copolymers. The goal of this study was to explore how fiber mesh stiffness affected endothelial cell shape, growth, migration, and angiogenic potential of endothelial cells. Furthermore, the effects of the E-modulus of fiber meshes on human adipose-derived stem cells (hADSCs) osteogenic potential was investigated.

Methods: Polyesteretherurethane (PEEU) polymers with various poly(p-dioxanone) (PPDO) to poly (ε-caprolactone) (PCL) weight percentages (40 wt.%, 50 wt.%, 60 wt.%, and 70 wt.%) were synthesized, termed PEEU40, PEEU50, PEEU60, and PEEU70, accordingly. The electrospinning method was used for the preparation of PEEU fiber meshes. The effects of PEEU fiber meshes with varying elasticities on the human umbilical vein endothelial cells (HUVECs) shape, growth, migration and angiogenic potential were characterized. To determine how the E-modulus of fiber meshes affects the osteogenic potential of hADSCs, the cellular and nuclear morphologies and osteogenic differentiation abilities were evaluated.

Results: With the increasing stiffness of PEEU fiber meshes, the aspect ratios of HUVECs cultivated on PEEU materials increased. HUVECs cultivated on high stiffness fiber meshes (4.5 ± 0.8 MPa) displayed a considerably greater proliferation rate and migratory velocity, in addition demonstrating increased tube formation capability, compared with those of the cells cultivated on lower stiffness fiber meshes (2.6 ± 0.8 MPa). Furthermore, in comparison to those cultivated on lower stiffness fiber meshes, hADSCs adhered to the highest stiffness fiber meshes PEEU70 had an elongated shape. The hADSCs grown on the softer PEEU40 fiber meshes showed a reduced nuclear aspect ratio (width to height) than those cultivated on the stiffer fiber meshes. Culturing hADSCs on stiffer fibers improved their osteogenic differentiation potential. Compared with cells cultured on PEEU40, osteocalcin expression and alkaline phosphatase (ALP) activity increased by $73 \pm 10\%$ and $43 \pm 16\%$, respectively, in cells cultured on PEEU70.

Conclusion: The mechanical characteristics of the substrate are crucial in the modulation of cell behaviors. These findings indicate that adjusting the elasticity of fiber meshes might be a useful method for controlling the blood vessels development and regeneration. Furthermore,

the mechanical characteristics of PEEU fiber meshes might be modified to control the osteogenic potential of hADSCs.

Zusammenfassung

Ziel: Das Verhalten von Endothelzellen oder mesenchymalen Stammzellen wird erheblich von den mechanischen Eigenschaften der Mikroumgebung beeinflusst. Hier wurden elektrogesponnene Fasernetze mit unterschiedlicher Elastizität aus Polyetheresterurethan (PEEU) hergestellt. Ziel dieser Arbeit war es, den Einfluss der Elastizität von Fasernetzen auf die Zellmorphologie, Proliferation, Migration und Angiogenese von Endothelzellen zu untersuchen. Außerdem war der Einfluss des E-Moduls von Fasersubstraten auf die Bindung an die Abstammungslinie von humanen Fettstammzellen (hADSCs) untersucht.

Methoden: Polyesteretherurethane (PEEU) mit unterschiedlichen Poly(p-dioxanon) (PPDO) to Poly (ε-Caprolacton) （PCL）-Gewichtsverhältnissen (40:60, 50:50, 60:40, 70:30) wurden synthetisiert und als PEEU40, PEEU50, PEEU60 bzw. PEEU70 bezeichnet. Die Fasernetze wurden durch Elektrospinnen von PEEU hergestellt. Dann wurden humane Endothelzellen der Nabelschnurvene (HUVECs) auf diesen elektrogesponnenen Fasernetzen aus Polyetheresterurethan (PEEU) kultiviert, die sich in ihrer Elastizität unterscheiden. Zellmorphologie, Proliferation, Migration und Angiogenese von Endothelzellen auf den abbaubaren Substraten wurden charakterisiert. Für den Einfluss des E-Moduls von Fasersubstraten auf die Bindung an die Abstammungslinie von hADSCs-Zellen und die Kernmorphologie wurde die Fähigkeit zur osteogenen Differenzierung bewertet.

Ergebnisse: Das Aspektverhältnis von HUVECs, die auf den Fasernetzen aus PEEU-Materialien kultiviert wurden, nahm mit zunehmender Steifheit der Materialien zu. HUVECs, die auf Fasernetzen mit hoher Steifheit (Young-Modul E = 4,5 ± 0,8 MPa) kultiviert wurden, zeigten eine höhere Proliferationsrate und eine signifikant schnellere Migrationsgeschwindigkeit sowie ein höheres Röhrenbildungsvermögen als die Zellen, die auf Fasernetzen mit niedriger Steifheit kultiviert wurden (E = 2,6 ± 0,8 MPa). Des Weiteren zeigten an steiferen PEEU70-Fasernetzen (PPDO: PCL = 70:30) gebundene hADSCs eine verlängerte Morphologie im Vergleich zu jenen, die auf weicheren Fasern kultiviert wurden. Das Kernaspektverhältnis (Breite gegen Länge eines Kerns) von hADSCs, die auf weicheren PEEU40-Fasern (PPDO: PCL = 40:60) kultiviert wurden, war niedriger als auf steiferen Fasern. Die osteogene Differenzierung von hADSCs wurde durch Kultivierung auf steiferen Fasern verstärkt. Im Vergleich zu PEEU40 wurde in Zellen auf PEEU70 eine 73 ± 10% ige Steigerung

der Osteocalcin-Expression und eine 34 ± 16% ige Steigerung der Aktivität der alkalischen Phosphatase (ALP) beobachtet.

Schlussfolgerung: Die mechanischen Eigenschaften des Substrats spielen eine Schlüsselrolle bei der Modulation des Zellverhaltens. Diese Ergebnisse deuten darauf hin, dass das Einstellen der Elastizität der Fasernetze eine potenzielle Strategie zur Modulation der Bildung oder Regeneration von Blutgefäßen sein könnte. Darüber hinaus könnte die Differenzierung von hADSCs durch die Anpassung der mechanischen Eigenschaften von elektrogesponnenen Fasern gestaltet werden.

Abbreviations and Symbols

%	Percentage
°	Degrees (Angles)
°C	Degrees Celsius (temperatures)
3D	Three dimensional
ALP	Alkaline phosphatase
BSA	Bovine serum albumin
CA	Contact angle
CD31	Platelet and endothelial cell adhesion molecule-1 (PECAM-1) or cluster of differentiation 31
ECs	Endothelial cells
ECM	Extracellular matrix
ELISA	Enzyme-linked immunosorbent assay
E-modulus	Young's modulus, Elastomeric modulus
et al.	et alii
EtO	Ethylene Oxide
FBS	Fetal bovine serum
$g \cdot mol^{-1}$	Gram per mole
GPC	Gel permeation chromatography
h	Hours
hADSCs	Human adipose-derived stem cells
HDI	Hexamethylene diisocyanate
HUVEC	Human umbilical vein endothelial cell
LDI	Lysine-based diisocyanate
min	Minutes
MMP	Matrix metalloproteinase
MPa	Megapascal
MSC	Mesenchymal stem cell
n	Number of samples
ng	Nanogram

OCN	Osteocalcin
PBS	Phosphate buffered saline
PCL	Poly(ε-caprolactone)
PPDO	Poly (p-dioxanone)
RUNX2	Runt-related transcription factor 2
SD	Standard deviation
SEM	Scanning electron microscopy
T	Temperature
TCP	Tissue culture plate
T_m	Melting temperature
T_g	Glass transition temperature
U	Unit
vs	Versus
v/v	Volume/volume
vWF	von Willebrand factor
w/v	Weight/volume
w/w	Weight/weight
wt.%	Weight percentage
ε	Strain
ε_b	Elongation at break
σ	Stress
µm	Micrometer

Note: the abbreviations listed above are singular, whereas any abbreviations present in the text ending with an 's' are plural. The polymer abbreviations starting with lowercase letter 'c' in the text present chemically cross-linked polymer networks

List of Figures

List of Tables

Chapter 1

Introduction

1.1 Biophysical cues modulate cell fate and function

Cells are encircled by both cellular and non-cellular factors, and cell behaviors are modulated by responses to the soluble and insoluble factors derived from their niche [1]. The important components of the cell niches include cell-cell interactions, cell-extracellular matrix (ECM) interactions, secreted factors, and biophysical cues [2, 3]. Biophysical signals comprise both extracellular-derived inputs and cell-generated responses that can be generally categorized into three categories: direct applications of mechanical force, just as fluid shear stress and cyclic strain; conventional biological stimuli, including soluble factors and adhesion molecules; physical properties of materials [4].
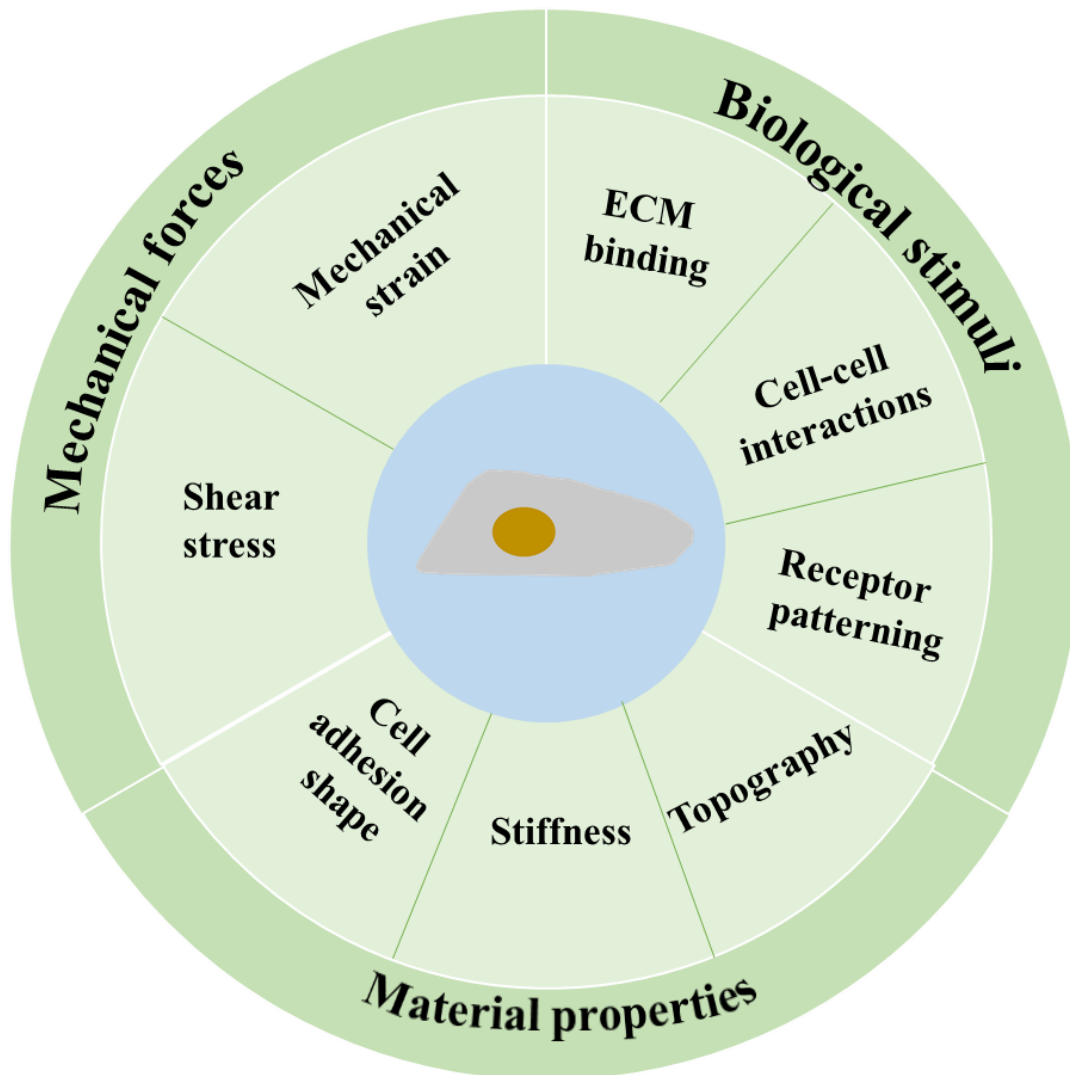
Figure 1-1 External biophysical factors regulate cell behavior and function.

The ECM's mechanical properties, including elasticity, actively participate in the modulation of cell function. The mechanical properties of the ECM also influence cell fate. Cells may perceive the ECM's mechanical signals, exert stress on it, and thereby further change the composition of ECM [5-8]. Interactions of cells and the ECM play a crucial role in the modulation of cell behaviors, such as viability, morphology, growth [9, 10], migration, and differentiation [10]. In addition, the mechanical properties of the ECM can be altered during pathological states, and can actively participate in the processes associated with disease progression and tissue homeostasis [11, 12].

1.2 Cellular mechanosensory processes

Cells can perceive, transmit signals, and answer to both dynamic and static mechanical stimuli through exerting traction tensions that mediate cell-ECM adhesions and alter downstream processes. The cell membrane contains diverse mechanosensitive molecules, for example, the integrin family, G protein-coupled receptors, stretch-activated ion channels, and growth factor receptors that activate various mechanotransduction pathways [13, 14]. The members of the integrin family are among the most widely investigated cell receptors and are known to mediate cell attachment and regulate various cellular behaviors [15]. Integrins perform their actions by selectively binding to ECM glycoproteins that have been deposited on the substrate surface, such as fibronectin, laminin, and collagen [16]. The specificity of integrin-ligand interactions is determined by various combinations of α and β subunit isoforms [15, 17], which form heterodimers that can detect extracellular stimuli. Mechanical stimuli can be transduced through both direct and indirect pathways that eventually reach the cell nucleus. Direct mechanotransduction signals are triggered as a result of mechanical loading and transfer information to the nucleus through the axis of ECM-integrin-cytoskeleton-nucleus, resulting in the activation of mechanosensitive genes [18]. Indirect pathways that are activated in response to mechanical stimuli involve multiple signaling cascades, resulting in the activation of Rac, Cdc42, mitogen-activated protein kinase (MAPK), and Rho/Rho-associated coiled-coil containing protein kinase (ROCK) [19].

It's been suggested that the nucleus can act as a cellular mechanosensor. Alterations in nuclear shape can cause conformational changes in chromatin structure and organization, which can cause the effects on transcriptional regulation, modulating cell growth or differentiation [20]. The ECM's mechanical forces can be detected by cells and delivered to the nuclear surface through the cytoskeleton. Because intracellular stress is balanced partly due to the nucleus, these mechanical forces can cause changes in the nuclear shape, suggesting that changes in the nuclear shape might be regulated by changes in substrate rigidity [21-24].

1.3 Modulation of stem cell' fates using polymeric biomaterials

Stem cells are tightly regulated by environmental niches, and changes in their microenvironments could dramatically influence their behaviors and differentiation capacities. Biomimetic scaffolds could potentially provide a controlled environment capable of directing

the attached cells' behaviors and differentiation capacities. Studies have explored methods to promote hADSCs' osteogenic differentiation by tuning the properties of biomimetic fiber meshes, which represents a potential approach for the restoration of bone defects.

Materials that feature suitable properties, such as specific surface topographies [25-31], that force a cell to form a certain shape [32-34], or varying degrees of stiffness [35-40], could be used to modulate cell fates. Increasingly sophisticated function-orientated materials are under development, including biomaterials with tunable mechanical properties [4].

1.3.1 General requirements of polymeric biomaterials

Biomaterials refer to substances that are designed to react with biological systems for medical purposes, such as the treatment, repair, or replacement of functional tissue within the body [41]. Currently, biomaterials are utilized for application containing regenerative medicine, controlled drug delivery systems, medical devices, and tissue engineering [42-45]. The general requirements of biomaterials [46] can be categorized as follows.

(1) Biomaterials and their degradation products should not be poisonous and should be able to be removed harmlessly from the human body to reduce unfavorable foreign body reactions after implantation.

(2) The degradation rate should match the rate of tissue regeneration.

(3) The mechanical characteristics of the biomaterials must be appropriate for the required task. Materials that feature mechanical features that are similar to those at the implanted sites can be beneficial for the preservation of structural stability and integrity, and they should provide suitable mechanical properties for implanted cells [47].

(4) Biomaterials should be easily tailored to match the requirements of the application task.

(5) Good biocompatibility is necessary. Biocompatibility influences cells adhesion, viability, migration, and proliferation, and poor biocompatibility may cause severe immune reactions and rejection following implantation.

Synthetic polymers feature tunable properties, including mechanical strength and erosion behaviors compared with natural polymers, such as collagen. Moreover, natural polymers may be associated with unwanted side effects. Therefore, biodegradable synthetic polymers have

been explored intensely to be used in tissue regeneration and nano-/micro-scale drug delivery systems [48].

In addition, the architecture of biomaterials is very important. The use of structures featuring innate interconnected pores and high porosity can ensure efficient nutrient diffusion to cells within the construct and via the ECM generated by these cells. A porous scaffold also allows for the diffusion of waste products produced by the cells.

1.3.2 Electrospun fiber meshes derived from biomaterials

Porous structures can be produced from various polymers using diverse processes, such as template synthesis, phase separation, self-assembly, melt blowing, and electrospinning [49-52].
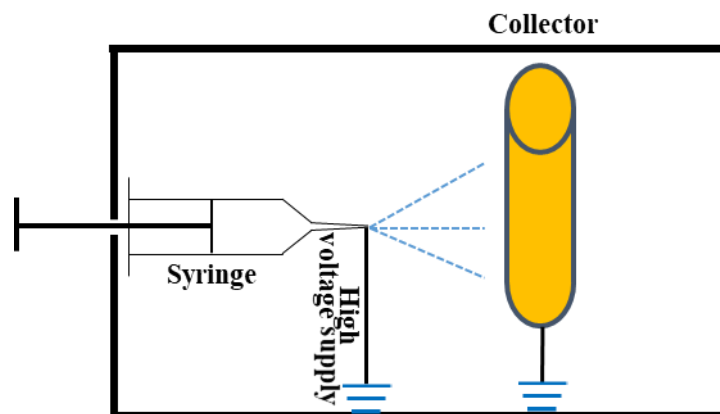
Figure 1-2 An electrospinning apparatus is depicted in a figure.

In comparison to other approaches, electrospinning is a simple, adaptable, and cost-effective for the production of fibrous structures [51]. The electrospinning machinery (as showed in Figure 1-2) primarily comprised of a syringe pump, a spinneret that is linked to a high-voltage power source, and a grounded collector [51, 53, 54]. Electrospinning can produce nano- and micro-fibers by employing an electric field to propel a jet of polymer solutions or polymer melts [55]. During the electrospinning process, a high voltage (usually 10-30 kV) is supplied to a polymer solution, which produces polymer melts or charged threads of polymer solutions at nano- or micro-fiber diameters.

Electrospinning can be used to produce fiber mesh scaffolds made from various polymer materials, such as synthetic polymers and natural proteins. Many fiber mesh scaffolds have been made from various polymers, including poly (ε-caprolactone) (PCL) [56, 57], and the

copolymer poly[(p-dioxanone)-co-(L-lactide)]-block-poly(ethylene glycol) [58]. Several fiber meshes fabricated using polymers have been used in blood vessel and bone tissue engineering. Previous studies have shown that electrospun fiber meshes derived from PCL materials are well-suited for bone tissue applications [59, 60]. Other studies have shown that scaffolds containing PCL, such as the starch: PCL (30:70 wt.%)-based fiber mesh scaffolds [61], PLLA- and PCL- based fibrous scaffolds [62], and PCL/PLA blend nanofiber scaffolds, are favorable for hMSC osteogenic differentiation [63]. Researchers have also fabricated fiber meshes from the copolymer poly[(L-lactid)-co-(ε-caprolactone)](75:25) and found that they were ideal tissue engineering scaffolds for blood vessel engineering [64, 65].

The production of fiber meshes using the electrospinning technique allows for the adjustment of scaffold features. Research has shown that the properties of fibers, such as morphology or thickness, and the final fiber mesh properties (size, shape, thickness, and porosity), can influence cell behaviors [66]. By partially mimicking the cellular microenvironment, the fiber network structure can provide relevant signals to modulate cell behaviors. In addition, fiber mesh scaffolds can be designed to resemble the human ECM, mimicking the ECM structure, which can be used to investigate the role placed by the ECM on cell behaviors. Scaffolds with fibers in the micrometer range have a high ratios of surface area to volume, which can enhance cell adhesion to the scaffolding material and is characterized by a high porosity that can be used to allow the passage of a wide range of proteins, like growth factors, enzymes, signaling molecules, and therapeutic drugs. The mechanical features of the fiber meshes should be designed to match those found at the implanted sites to preserve the structural integrity of the implanted sites, establishing an appropriate mechanical environment for the implanted cells. These factors could be adjusted [67] to modulate cell behaviors, such as cell adhesion, spreading, proliferation, and differentiation [68].

1.4 PDC and PEEU copolymers

PCL is a biocompatible, absorbable synthetic polymer. PCL with a high molecular weight is synthesized by ε-caprolactone's ring-opening polymerization. The mechanical features of PCL make it appropriate for a variety of applications. The PCL polymer is widely used as an implantable biomaterial in various devices that have been approved by the Food and Drug Administration (FDA) for current clinical applications during specific applications within the human body. Poly(p-dioxanone) (PPDO) has also demonstrated suitable biocompatibility and

mechanical features, which are likely to be suitable for a multitude of applications in the medical industry [69].

The degradation time of synthetic biomaterials should match the time of regeneration or required treatment, and the mechanical features of the biomaterial must be appropriate for the required task. The use of a copolymer allows for the tuning of the degradation rate, host compatibility, and mechanical properties.

At our institute, a copolyetheresterurethane multiblock copolymer (PDC) was previously synthesized, containing PPDO segments and PCL segments. Low molecular weight diisoyanate was employed to combine the polymer blocks via urethane linkages. In the end, products with an average molecular weight of more than 10^5 g·mol^{-1} were obtained. The degradability and thermal and mechanical properties of PDC are adjustable by varying the molecular parameters. Lowering the PPDO (hard segments) weight percentage reduced the polymer's E-modulus and increased the elongation of polymer. Because PDC has a very low glass transition temperatures, biomaterials generated from it forming elastic materials at body temperatures.

Fiber meshes of PDC, in contrast to rigid films, behave like a textile and may conform to the curvature of tissues found at the implantation site. Tensile tests results of PDC films demonstrated a low stiffness (E-modulus = 20 ± 1 MPa) and a high elongation at break (ε_b = 420 ± 30%) [70], whereas the electrospun scaffolds were characterized by an increased Young's modulus (E-modulus = 50 ± 10 MPa) and a reduced deformability value (ε_b = 210 ± 30%) [71]. PDC was characterized as a hydrophilic material both in the form of flat films and fiber meshes scaffolds, with water contact angles of 63 ± 4° and 56 ± 5° (PDC$_{ran}$) [70]. PDC is a shape-memory multiblock copolymer that is flexible and biodegradable. PDC was found to undergo linear mass loss in both enzymatic degradation and hydrolytic experiments. The pace of degradation may be adjusted by modifying the weight ratio between PPDO and PCL in the polymer and by changing the surface to volume ratio of the scaffold [72, 73].

PDC shows a cell-selective adhesion ability *in vitro*. PDC is able to selectively enhance the adhesion of ECs whereas inhibiting the attachment of smooth muscle cell, both as film materials and as fiber meshes scaffolds [70, 71], which indicated that PDC might offer a great replacement for the restoration of blood vessels [70, 71].

PDC films might possess an angiogenic potential *in vivo*, and PDC has been shown to stimulate the formation of new blood vessels in close proximity to implanted tissues in the rat neck and in the chorioallantoic membranes of chicken eggs [74, 75].

In summary, PDC is a viscoelastic and flexible polymer with a low T_g, which is better for a possible implant. The adjustable biodegradability, changeable mechanical features, low thrombogenicity [76], the ability to selectively enhance the adhesion of ECs [70, 71], and pro-angiogenic properties[74, 75] contribute to the characterization of PDC as a desirable implant candidate for blood-contact usages, vascular implants or EC selective' devices, for example.

In this thesis, a multi-block copolymer, PEEU, composed of PPDO and PCL segments using lysine-based diisocyanate (LDI) linkers, was synthesized using the previously described method for the generation of PDC, which was a PEEU generated using hexamethylene diisocyanate (HDI) linkers. Fiber meshes scaffolds were synthesized using an electrospinning method. Hopefully, these scaffolds could act as a supporting matrix for bone tissue engineering, directing mesenchymal stem cells to differentiate into osteoblast cells and promoting angiogenesis of endothelial cells to form blood vessels.

1.5 Cells needed in bone regeneration

Hence, biomimetic fibrous scaffolds with defined stiffness could modulate hADSCs and HUVECs behaviors to promote their capacity for bone regeneration, and improve vascular and bone regeneration in the human body following transplantation.

1.5.1   Human umbilical vein endothelial cells (HUVECs)

Endothelial cells (ECs) are mesoderm-derived cells that comprise the endothelium, a one-cell thick layer that lines all blood vessels [77]. HUVECs are the most widely employed human EC type because they're easily accessible, devoid of known pathological processes and are physiologically relevant compared with numerous others established cell lines.

ECs participate in various physiological processes, such as hemostasis, blood vascular tone, inflammation, angiogenesis, and wound healing [78]. ECs are typically continually exposed to different mechanical factors, including shear force and the stiffness of blood vessel. ECs can

perceive mechanical stimuli and modulate the organization of the actin cytoskeleton's structure in an integrin-dependent way to transmit mechanical forces into meaningful cellular functions, including angiogenic potential [79-83].

1.5.2   Human adipose-derived stromal cells

Mesenchymal stem cells (MSCs) are a multipotent stem cell type, with the capability for self-renewal, and the potential to differentiation into a variety of cell types, containing adipocytes, chondrocytes, and osteoblasts [84]. Hence, MSCs could be used for the renewal of various mesenchymal tissues, containing adipose tissue, muscle, cartilage, and bone. MSCs were originally found out in bone marrow and can now be easily acquired from a variety of mesenchymal tissues, containing adipose tissue and skeletal muscle [85]. Adipose tissue represents an appealing supply for MSCs, because adipose tissue is abundant and readily accessible using routine liposuction procedures, which are typically associated with minimal morbidity [86-88]. hADSCs have been reported in applications designed to maintain the integrity of bone, cartilage, and other tissues. hADSCs expand rapidly, can sustain their differentiation potential when grown *in vitro* cultures, and are currently extensively utilized in preclinical and clinical studies. In addition, hADSCs have been reported to undergo osteogenic differentiation in response to minimal stimulation by exogenous cytokines and are considered as a promising way for skeletal repair.

As mentioned above, hADSCs can differentiate into various mature mesenchymal cell types, containing adipocytes and osteoblasts. A range of signaling pathway and transcription factors are involved in the differentiation of hADSCs into adipocytes or osteoblasts, and several researches have reported an inverse relationship between adipogenic and osteogenic differentiation, indicating that the upregulation of osteogenic differentiation factors is associated with the downregulation of adipogenesis and vice versa (Figure 1-3) [89, 90].
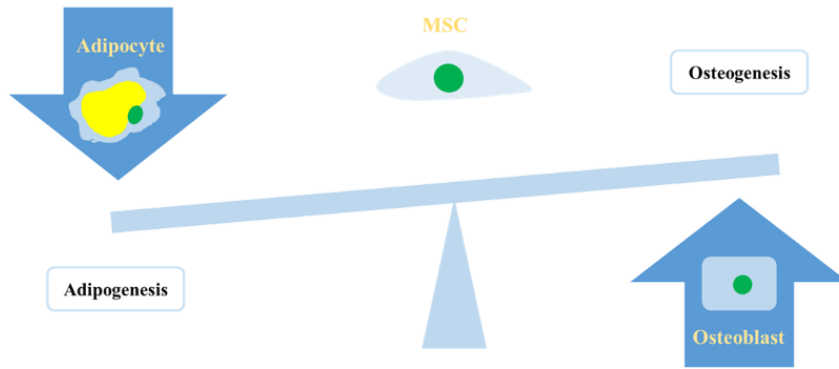
Figure 1-3 Reverse correlation between osteogenesis and adipogenesis.

Bone consists of a specialized cell type, osteoblasts, and the remodeled surrounding ECM, which contains collagen type I, osteocalcin (OCN), osteopontin, and mineralized matrix or hydroxyapatite. The molecules that control the osteogenic differentiation of mesenchymal cells have been carefully investigated, and RUNX2/CFBα1, a helix-loop-helix nuclear factor, has been found to initiate the osteogenic differentiation of MSCs. Alkaline phosphatase (ALP) is also highly expressed during osteogenic differentiation, and OCN is highly expressed during the late osteogenesis stage [91] (Figure 1-4).
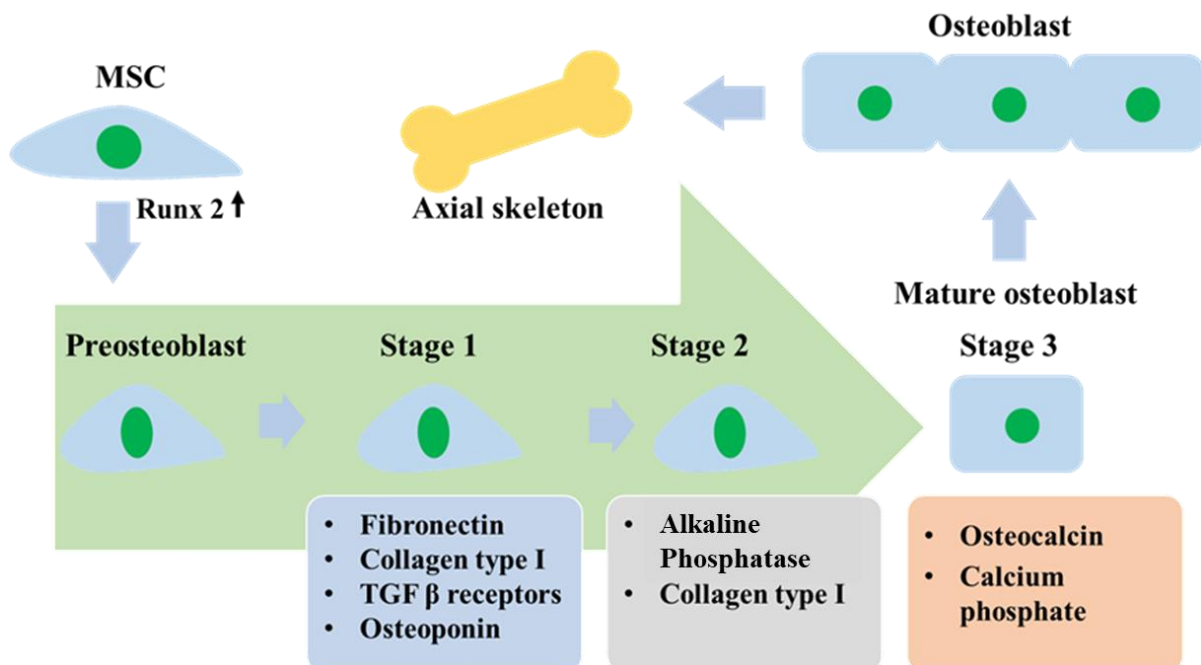
Figure 1-4 The biogenesis of osteoblasts is described in a schematic.

Chapter 2

Motivation and Aims

An ideal biomaterial for tissue engineering applications should possess good biocompatibility, be nontoxic, feature an appropriate level of biodegradability, and have suitable mechanical properties to promote cell adhesion, growth, and differentiation, while simultaneously avoiding the initiation of host immune responses [92, 93].

The degradability, the thermal properties, and mechanical features of PDC were previously shown to be adjustable through the variation of molecular parameters. These materials are elastic at room temperature and exhibit excellent elongation properties. A stiffer polymer could be obtained by increasing the quantity of PPDO. PEEU is a similar material to PDC, except a much better biocompatibility linker, LDI. LDI-based polyurethanes (PEEU) have been characterized with reduced cytotoxicity and better hemocompatibility than HDI-based polyurethanes (PDC) [94]. Additional hydrogen bonding groups (carbonyl and ester oxygen atoms) on the ethyl ester side group of LDI may additionally contribute to LDI-based polyurethanes' hydrophilicity [95], which could promote the adhesion of cells .

Fabricated three-dimensional (3D) scaffolds are more biomimetic than two-dimensional (2D) substrates because the cells are exposed to 3D microenvironments *in vivo*. Moreover, the scaffolds in near-physiological environments were found to possess desirable mechanical properties, high porosity, and physical stability, which could be used to modulate cell attachment, proliferation, development, and differentiation toward preferred lineages [96]. This research examined four PEEU compositions featuring various PPDO proportions ranging from 40 wt.% to 70 wt.%, which were referred to as PEEU40, PEEU50, PEEU60, and PEEU70. The scaffolds were fabricated using the electrospinning method to mimic the ECM's native components and structural features [97-99]. Electrospun fiber meshes feature a 3D structure with an interconnected pore system.

The limited availability of fibrous scaffolds that are similar to the natural ECM in blood vessels has limited the exploration of the physiological responses of ECs to the ECM and the exploration of the mechanisms that underly mechanical perceiving and the associated

downstream pathways in ECs. Understanding of how proper physical signals are employed to govern the angiogenesis process is crucial to controlling a range of favorable cellular processes to promote regeneration [100, 101]. Furthermore, understanding the physical signals that govern angiogenesis may assist in the development of desired biological structures capable of restoring normal EC functions in wounded tissues or organs while inhibiting pathological angiogenesis, such as that occurs during tumor growth [102]. The findings of this study will aid in a better understanding the effects of the *E*-modulus of fiber meshes on the therapeutic efficiency of EC implantations and facilitate the design of more suitable scaffolds, featuring optimal *E*-modulus characteristics, to increase the regenerative potential of these biomaterials.

In addition, loss or dysfunction of skeletal tissue as a result of trauma, injury, disease or ageing can result in considerable morbidity and is associated with enormous economic costs [103]. Currently, clinical treatments for bone repair and restoration typically focus on bone transplantations, including the gold standards of autografts and allografts. Bone transplantation methods are faced with several challenges, including considerable donor shortages, donor site injuries, and morbidity, resulting in substantial limitations on these procedures [104]. In recent years, researches have attempted to meet the urgent need for bone augmentation and skeletal repair by using new approaches to skeletal tissue formation. These studies have aimed to combine stem cells and tissue-mimicking scaffolds with specific lineage-inducing biological factors to design new robust, and reproducible methods for the enhancement of bone formation.

This research could combine to our understanding of which cell types can be easily obtained and differentiated into bone tissue, and what types of fiber meshes can be used to promote these cells to differentiate into bone. Furthermore, the findings of this study could better inform the design of biomaterials featuring the optimal stiffness for the promotion of hADSCs toward osteogenic differentiation.

In summary, the aims of this project were as follows:

1) Four types of multi-block copolymer PEEU, composed of different PPDO and PCL segments using LDI as a linker were synthesized. The PPDO weight ratio was varied among 40 wt.% and 70 wt.%. The mechanical properties of PEEU can be adjusted with the variation of PPDO composition.

2) The characteristics of fiber mesh scaffolds generated using the four PEEU materials in combination with the electrospinning method were examined, to optimize several key

parameters of the electrospinning method to produce fiber meshes with similar fiber diameters and porosity as ECM.

3) Fiber mesh scaffolds derived from the multiblock copolymers featuring various elastic properties were developed, and their effects on EC behaviors were examined, including cell morphology, growth, migration, and tube formation ability.

4) The effects of fiber mesh scaffolds featuring various elastic properties on the differentiation of hADSCs into osteogenic lineages were examined, including how the mechanical properties of the meshes affected hADSCs morphology.

Chapter 3

Hypotheses, Concept, and Strategies

Hypotheses and Concept

PEEU copolymers were synthesized using LDI as a linker instead of the HDI used in PDC and the mechanical features of PEEU can be adjusted by changing the PPDO proportion, with increased PPDO proportions associated with the formation of a stiffer polymer. Therefore, we hypothesized that PEEUs would possess good biocompatibility, be non-toxic, display the proper biodegradability characteristics, and feature suitable mechanical characteristics to promote cell adhesion, growth, and differentiation, which would suggest that PEEUs represent ideal biomaterials for use in human body implantations during tissue engineering applications.

Microfiber mesh scaffolds capable of mimicking the natural ECM can contribute to cell proliferation. In addition, these scaffolds feature large surface areas, which would be beneficial for cell attachment and extracellular protein deposition. Hence, microfiber mesh scaffolds were fabricated to adjust cell adhesion and growth for applications in regenerative medicine.

Differences in the E-modulus of fiber meshes can influence cell behaviors. We hypothesis that HUVECs are influenced by their culturing microenvironment, and are capable of sensing and responding to the mechanical features of PEEU fiber mesh scaffolds; therefore, variations in the E-modulus values of fiber meshes could influence EC attachment, morphology, proliferation, and tube formation abilities. The increased stiffness of fiber meshes could also induce integrin accumulation and activation in hADSCs, elongating the cell morphology, causing the elongation of the nucleus and promoting the differentiation of hADSCs into osteogenic cell lineages.

In Section 4.2, The effects of alterations in EC substrate stiffness on the angiogenesis process of HUVECs, which are generated from the endothelium of veins in the umbilical cord, were investigated using an in vitro model of the vascular endothelium. HUVECs are used to examine the function and pathophysiology of ECs *in vitro* (e.g. angiogenesis) [83]. HUVECs can sense physical signals from their surroundings, such as elasticity, which resulting in changes in cell

29

functions. The impact of substrate elasticity on HUVEC functions were investigated by culturing HUVECs on electrospun PEEU fiber meshes containing various elasticities. The effects of varying substrate elasticities on cell morphologies were carefully studied. We further studied whether PEEU-derived fiber meshes with different elasticities influence other EC behaviors, such as migration, proliferation, and angiogenesis.

In Section 4.3, the effects of fiber mesh stiffness on hADSC behaviors were examined by culturing hADSCs on electrospun PEEU fiber meshes. Changes in cell morphologies were carefully examined to determine the influences of varying the mechanical features of the fiber meshes on the osteogenesis of hADSCs.

Strategies

The goal of this research was to identify polymers with good biocompatibility to meet the requirements for use in potential implantation and tissue restoration applications. A polymer was fabricated, named PEEU, using LDI as the linker instead of the HDI linker used in the previously studied polymer, PDC. LDI shows better biocompatibility than HDI; therefore, PEEU was chosen as the polymer material for this study. PEEU multiblock copolymers containing PPDO and PCL segments were fabricated, with four different weight percentages of PPDO: PCL (w/w), and the PPDO proportion ranging from 40 wt.% to 70 wt.%.

Electrospinning can be used to produce fiber mesh scaffolds from polymeric solutions and allows for the adjustment of various scaffold features, including the mechanical properties of the fibers and fiber morphology and thickness. Hence, the electrospinning technique was selected in this project for the production of the four different types of PEEU fiber meshes. Uniform diameter microfibers meshes were generated by controlling the electrospraying parameters, including the polymer solution concentration, the mass flow rate, and humidity. The resulting fiber meshes were sterilized with ethylene oxide 10% (v/v) at 54 ℃, 1.7 bar pressure, 65% relative humidity, and 3 hours of gas exposure time, followed by 21 hours of aeration phase to allow for the applications of the scaffolds in sterile cell cultures.

To characterize the properties of the fiber meshes, SEM was carried out to characterize the morphologies and the fiber diameter distributions of the generated PEEU fiber meshes. A tensile strength testing experiment was used to measure the mechanical properties of the generated PEEU fiber meshes.

To verify the hypothesis that varying the stiffness of the fiber mesh could influence EC behaviors, HUVECs were cultured on PEEU fiber mesh scaffolds with different elasticities. After overnight cultivation, enabling the cells to fully attach to the scaffolds, the scaffolds and attached cells were transferred into a new well containing fresh culture medium (as shown in Figure 3-1). The viability, cell shape, growth, migration, and angiogenic potential of cells cultured on the varied stiffness of fiber meshes were examined.

To evaluate the influence of fiber mesh stiffness on hADSC behaviors, fiber mesh scaffolds generated using PEEU40, PEEU50, PEEU60, and PEEU70 were used to evaluate cell behaviors. hADSCs were seeded onto the fiber meshes, and after overnight cultivation, the fiber meshes and associated cultured cells were transferred into a new well (as shown in Fig.3-1). The viability, cell attachment, cell shape, and nuclear aspect ratios of the cells cultured on the fiber mesh substrates were evaluated. Cells were seeded with a high density to perform the osteogenic differentiation experiment. First, the cell densities on each fiber mesh substrate were measured. Then, cells osteogenic differentiation was initiated by the addition of osteogenic differentiation medium. The expression levels of the osteogenesis related protein RUNX2, OCN, and the activity of bone-specific ALP were measured to assess the osteogenesis potential of hADSCs cultured on the fiber meshes. Finally, matrix mineralization was evaluated by measuring the levels of the late-stage osteogenic differentiation marker, hydroxyapatite using fluorescence staining.
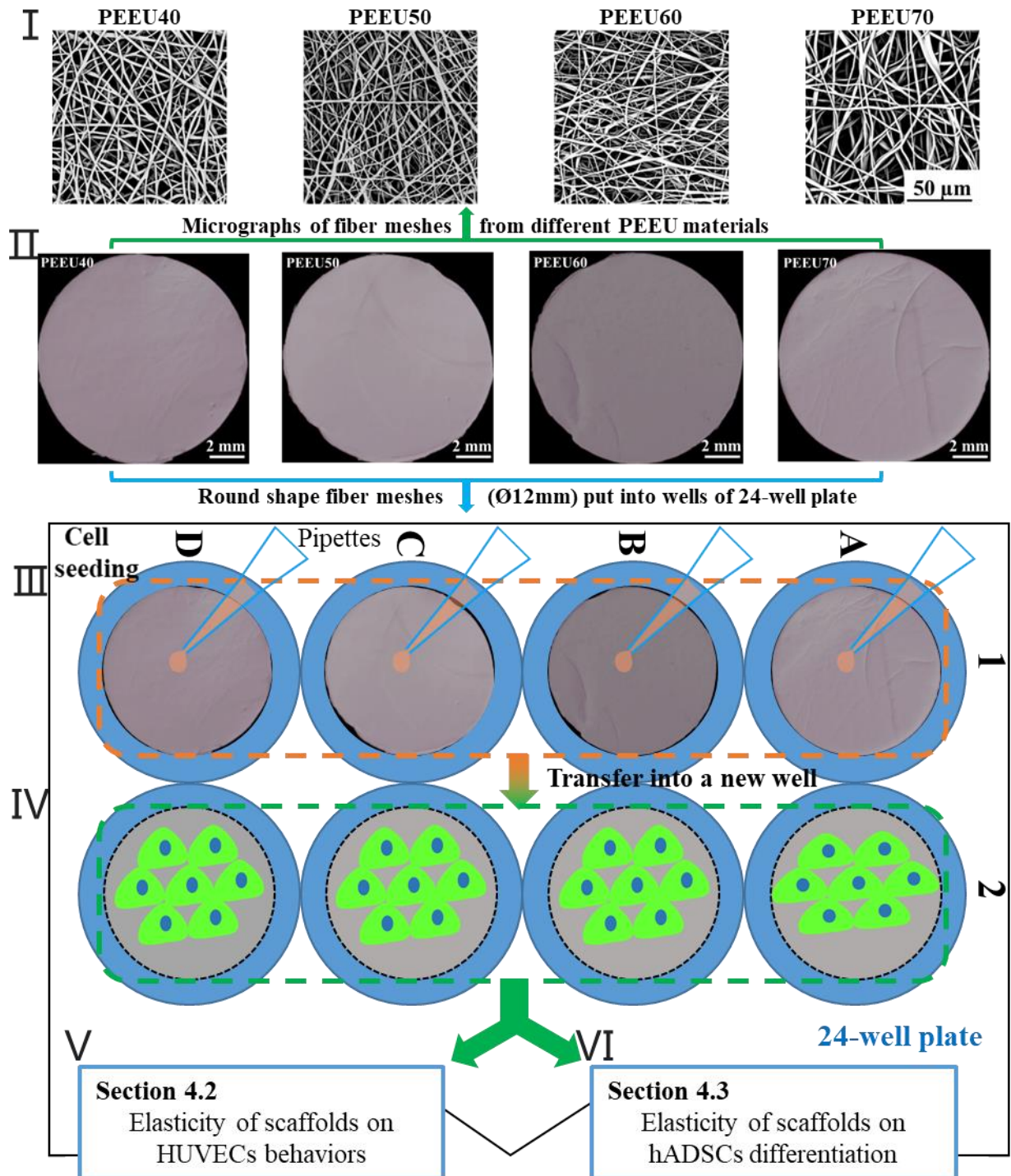
Figure 3-1 Scaffolds preparation and study design. (I) Micrographs of PEEU scaffolds. (II) Scaffolds were punched into a round shape with a diameter at 12 mm. (III) Scaffolds were put into wells of 24-well plate and cells were seeded onto them with proper density. (IV) Scaffolds incorporating with cells were put into new wells for the following experiments. (V) and (VI) Elasticity of scaffolds on HUVECs behaviors in **Section 4.2** and hADSCs osteogenic differentiation in **Section 4.3**.

Chapter 4

Results and Discussion

4.1 Characteristics of PEEU fiber meshes

4.1.1 Molecular weights of PEEU multiblock copolymers

A multiblock copolymer (PEEU) was developed, composed of PPDO and PCL segments and using LDI as the linker. The multiblock polymers were provided by Dr. Karl Kratz, Dr. Michael Zierke, and Monique Hannemann at our institute. The proportion of PPDO varied between 40 wt.% to 70 wt.%. Four different PEEU materials were synthesized, using the method illustrated by Kratz et al. [73] and Grablowitz and Lendlein [105]. Figure 4-1 depicts the chemical structure of the PEEU material.
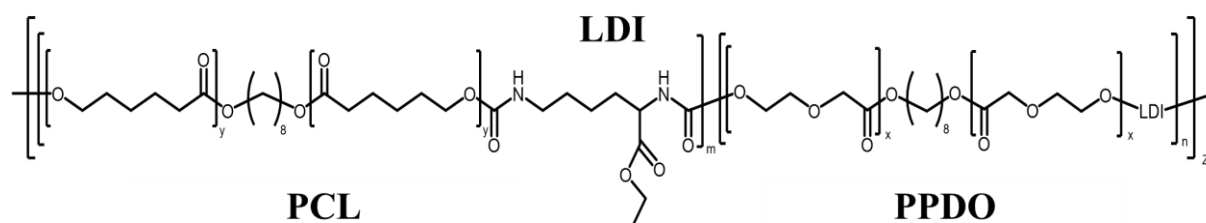
Figure 4-1 Chemical structure of the PEEU multiblock copolymer.

The molecular weights and polydispersity index values of were measured by gel permeation chromatography (GPC), using trichloromethane as the solvent and polystyrene as a standard. Dr. Michael Zierke performed this characterization at our institute. The weight-average molecular weights (M_w) of PEEU40, PEEU50, PEEU60, and PEEU70 were 91 kg·mol^{-1}, 82 kg·mol^{-1}, 88 kg·mol^{-1}, and 134 kg·mol^{-1}, respectively. In addition, their polydispersity index values were 1.9, 2.5, 2.4, and 2.2, respectively (Table 4-1). The results were consistent with those of a previous research [106].

Table 4- 1 Molecular weights (GPC) of PEEU materials

	Composition [a] PDDO : PCL	M_n [b] (g/mol)	M_w [c] (g/mol)	M_p [d] (g/mol)	D [e]
PEEU40	40 : 60	47000	91000	97000	1.9
PEEU50	50 : 50	33000	82000	88000	2.5
PEEU60	60 : 40	37000	88000	92000	2.4
PEEU70	70 : 30	61000	134000	112000	2.2

[a] Copolymer composition in weight %.
[b] Number-average molecular weight (M_n).
[c] Weight-average molecular weight (M_w).
[d] Molecular weight at the highest point of the peak.
[e] Polydispersity index (M_w/M_n) determined by GPC.

This table was generated for this thesis according to the characterization data. GPC: gas permeability chromatography; Polyetheresterurethane, PEEU; Poly(*p*-dioxanone), PDDO; Poly(*ε*-caprolactone), PCL; polydispersity index value, D.

4.1.2 Thermal properties of PEEU materials

The thermal characteristics of the PEEU multiblock copolymers were measured using differential scanning calorimetry (DSC). The DSC thermogram of PEEU materials are shown in Figure 4-2 and the thermal properties, showed in Table 4-2, were calculated from the second heating curve. For all prepared PEEU materials, the melting temperature of PCL was between 39.3 °C and 45.1 °C (Table 4-2). Therefore, the PCL remained in a solid state during the planned trials which were performed at 37 °C.

The thermal properties of PEEU polymer scaffolds were examined in the previously reported study [106]. The multiblock copolymer PEEU exhibited glass transitions (T_g) at -14 °C, which was associated with the presence of the PPDO segments, and two melting transition temperatures (T_m), observed at 41 and 92 °C, were associated with the PCL and PPDO segments, respectively [106], which were similar to the previously reported results for PDC [73].
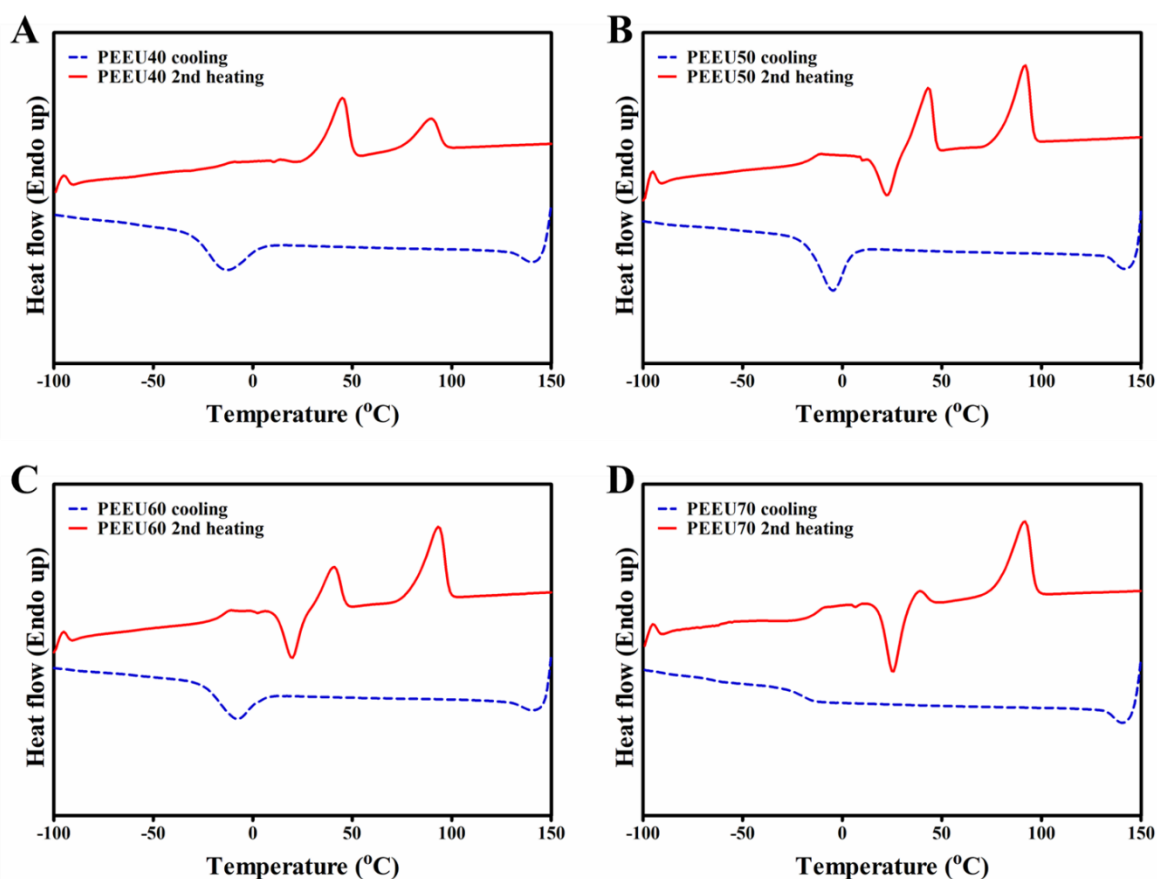
Figure 4-2 DSC thermogram of PEEU materials: second heating curve (solid red line) and cooling curve (dotted blue line). DSC thermogram of PEEU40 (A), PEEU50 (B), PEEU60 (C), and PEEU70 (D) were showed respectively.

Table 4-2 Thermal properties of PEEU materials

	$T_{g, PDDO}$ (°C)	$T_{m, PCL}$ (°C)	En_{PCL} (J/g)	$T_{m, PPDO}$ (°C)	En_{PPDO} (J/g)
PEEU40	-13.3 ± 0.5	45.1 ± 0.5	2.4 ± 0.1	89.7 ± 0.5	16.5 ± 0.2
PEEU50	-15.0 ± 0.5	43.3 ± 0.5	13.9 ± 0.1	91.7 ± 0.5	30.0 ± 0.3
PEEU60	-14.8 ± 0.5	40.9 ± 0.5	15.8 ± 0.2	93.3 ± 0.5	31.3 ± 0.3
PEEU70	-14.0 ± 0.5	39.3 ± 0.5	21.5 ± 0.2	91.7 ± 0.5	33.2 ± 0.3

4.1.3 Fiber diameter variation of the PEEU fiber meshes

The morphologies of PEEU40, PEEU50, PEEU60, and PEEU70 were examined using SEM. Figure 4-3 (A) shows the SEM images for the various PEEU scaffolds. A histogram showing the average fiber diameter distribution, according to the analysis performed on the fiber mesh

SEM images, can be observed in Figure 4-3 (B). Average fiber diameters (shown as mean ± SD) of the fiber meshes originates from PEEU40, PEEU50, PEEU60, and PEEU70 were 1.7 ± 0.5 µm, 1.4 ± 0.6 µm, 1.4 ± 0.5 µm, and 1.7 ± 0.4 µm, accordingly. No significant differences in fiber diameters were observed among the groups. Micron scale fibers (2 µm) of PDC were determined to represent promising candidate materials for blood-contact biomaterial applications compared with submicron-scale fibers (0.5 µm) [107]. HUVECs cultured on micron-scale fibers displayed increased adhesion and improved proliferation and viability compared with HUVECs cultured on submicron-scale fibers [107]. Therefore, the PEEU scaffolds generated in this study featuring micron-scale single fibers (1.4 – 1.7 µm) may also represent promising candidate materials for the support of HUVEC attachment and proliferation.
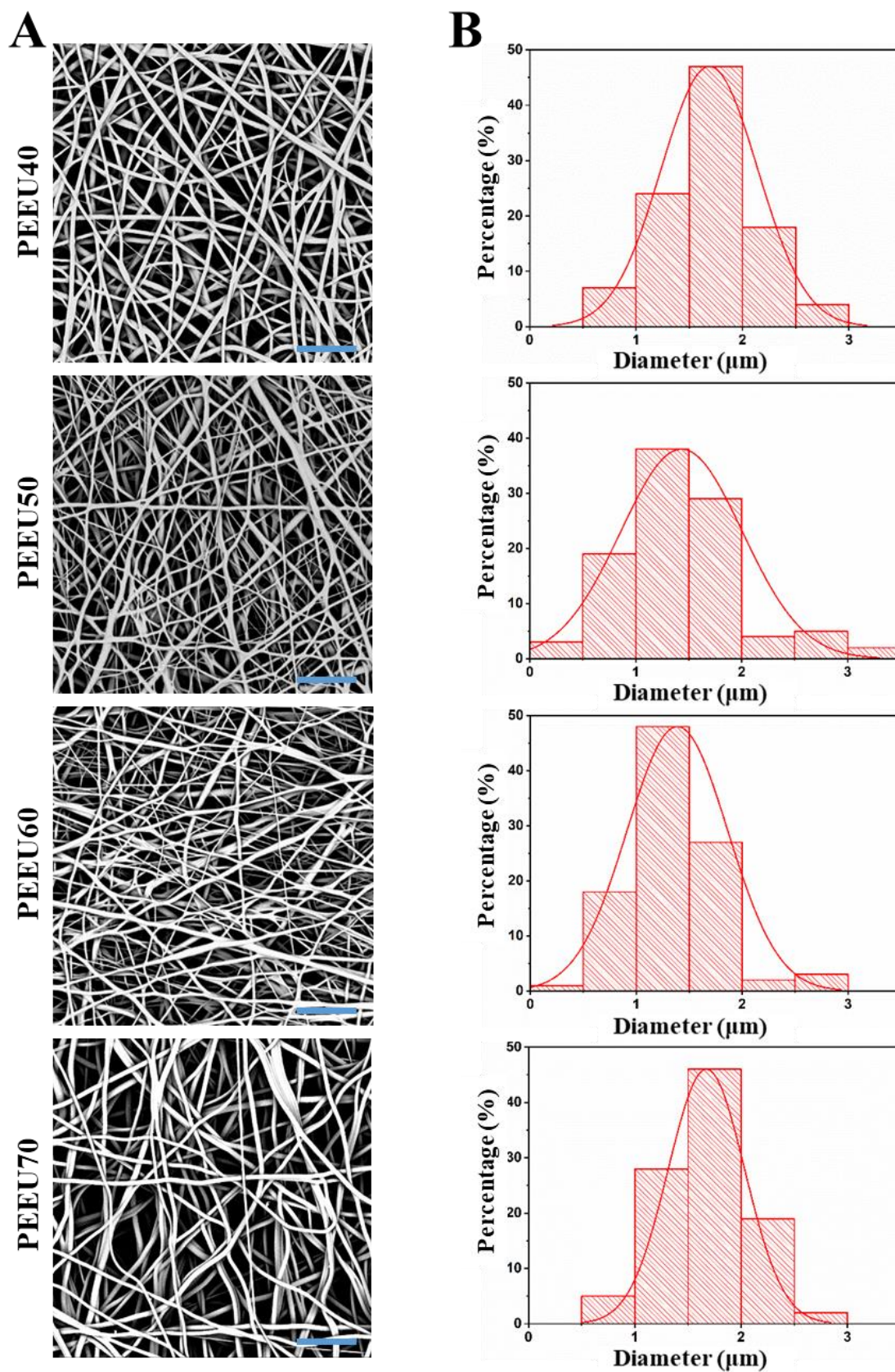
Figure 4-3 SEM micrographs of PEEU fiber meshes (A) and associated diameter distributions (B), showing the distributions of fiber diameter measured in all PEEU fiber meshes. The scale bar is 25 µm.

4.1.4 The modulus of elasticity of PEEU fiber meshes

Figure 4-4 shows stress-strain curves acquired during the tensile tests of the fiber mesh derived from PEEU materials, which were conducted at 37 °C under dry conditions.
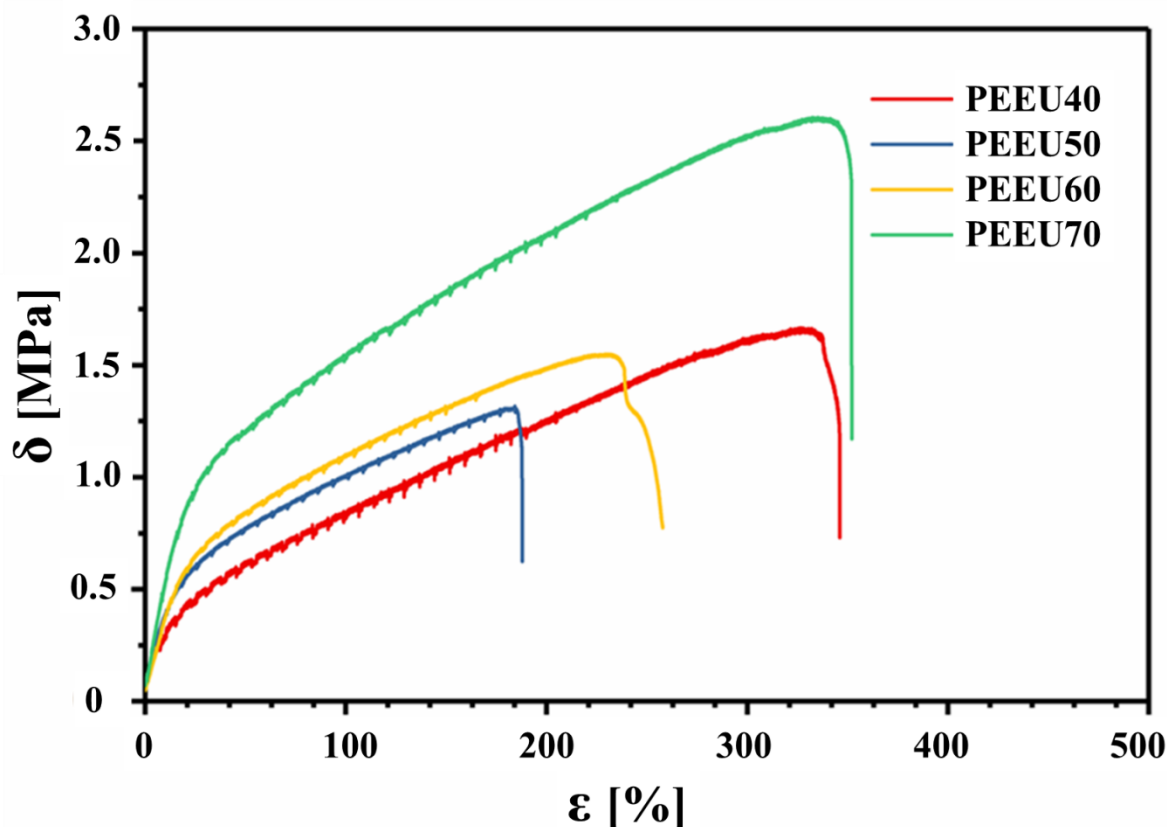
Figure 4-4 Stress–strain curves for fiber meshes derived from PEEU40 (blue line), PEEU50 (orange line), PEEU60 (grey line), and PEEU70 (yellow line).

In addition, the mechanical features are showed in Table 4-3. The elasticity values of the PEEU fiber meshes rose from PEEU40 to PEEU70, as the PPDO composition increased, indicating that the elasticity is probably associated to the weight content of PPDO (hard segments) within the fibers. The *E*-modulus of PEEU70 fiber meshes is higher than that of PEEU40 fiber meshes (showed in Figure 4-5). The elongation values of all of the tested PEEU fiber meshes were above 150%, which is consistent with the previously reported data [106]. In contract, the *E*-modulus of the PDC50 scaffold was 51 ± 8 MPa [72], compared with the average *E*-modulus of approximately at 4 ± 1 MPa of the PEEU scaffolds examined here. This difference may be a result of the higher number-average molecular weight of 75 kg·mol^{-1} observed for PDC,

compared with the values obtained for the various PEEU compositions, and the use of a different conjugate linker.

Table 4-3 Mechanical characteristics of the investigated fiber meshes generated from PEEU materials, as determined by a tensile test performed in air at 37 °C.

	E-Modulus (MPa)	Failure stress (MPa)	Elongation at break (%)	Mesh thickness (µm)
PEEU40	2.6 ± 0.8	1.4 ± 0.4	320 ± 110	39.3 ± 2.7
PEEU50	3.2 ± 0.9	1.1 ± 0.2	150 ± 15	87.3 ± 10.0
PEEU60	4.0 ± 0.9	1.6 ± 0.1	270 ± 10	77.8 ± 3.9
PEEU70	4.5 ± 0.8	2.8 ± 0.2	410 ± 50	53.8 ± 3.9
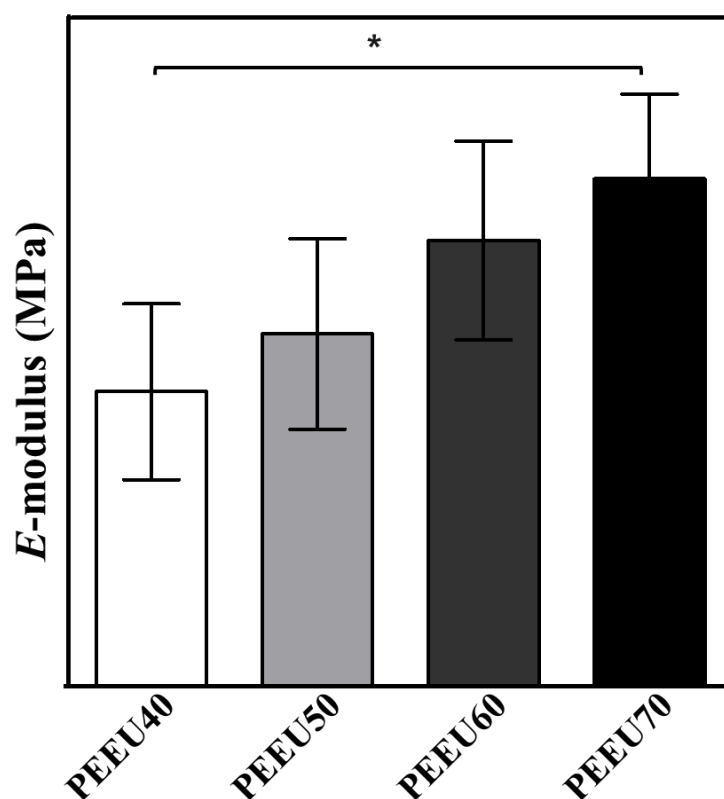
Figure 4-5 *E*-modulus quantification of PEEU scaffolds (n $_{PEEU40}$ = 8; n $_{PEEU50}$ =7; n $_{PEEU60}$ = 4; n $_{PEEU70}$ = 4). Results are expressed as mean ± SD. One-way ANOVA with Tukey's multiple comparisons test was used to statistically analyze the data. $p < 0.05$, *. Results are expressed as mean ± SD.

In summary, the parameters of electrospinning method were optimized to achieve the production of scaffolds that featured similar diameters (approximately 1.5 µm) and porosity values (60%) [106]. Micron-scale fibers in high porosity scaffolds contribute to cell attachment and proliferation. The glass transition temperatures are below body temperature and two melting transition temperatures (T_m), were all observed above 37°C. Therefore, the PEEU scaffolds were characterized as being soft and elastic materials, representing promising candidates for use in body implantation applications. The PEEU scaffolds showed increasing stiffness with the increasing incorporation of PPDO segments, and the E-modulus for PEEU70 was significantly higher than that of PEEU40, which may influence cells behaviors.

4.2 Endothelial cell activity is modulated by the elasticity of PEEU fiber meshes

In this section, an *in vitro* model of the vascular endothelium was used to explore the effects of fiber meshes stiffness on angiogenesis in ECs. HUVECs, which are generated from the endothelium of umbilical cord veins, can be employed to provide an in vitro model for studying the ECs function (e.g. angiogenesis). The effects of PEEU scaffold elasticity on HUVEC behaviors were investigated, and the morphology, migration, proliferation, and angiogenesis of cells grown on PEEU scaffolds were carefully studied.

4.2.1 Characterization of HUVECs

HUVECs were successfully cultured according to the provided protocol of the used medium. The cells were homogenous with indistinct cell borders. They showed a typical cobblestone form, which is typical pattern of ECs (Figure 4-6A). CD31 (cluster of differentiation; also known as platelet and endothelial cell adhesion molecule-1, PECAM) and vWF (von Willebrand factor) are considered to be good EC biomarkers [108, 109]. The cultured HUVECs were higher than 95% of CD31- and vWF- positive, as detected using a flow cytometric assay (Figure 4-4B), indicating the high purity of HUVECs in our culture.
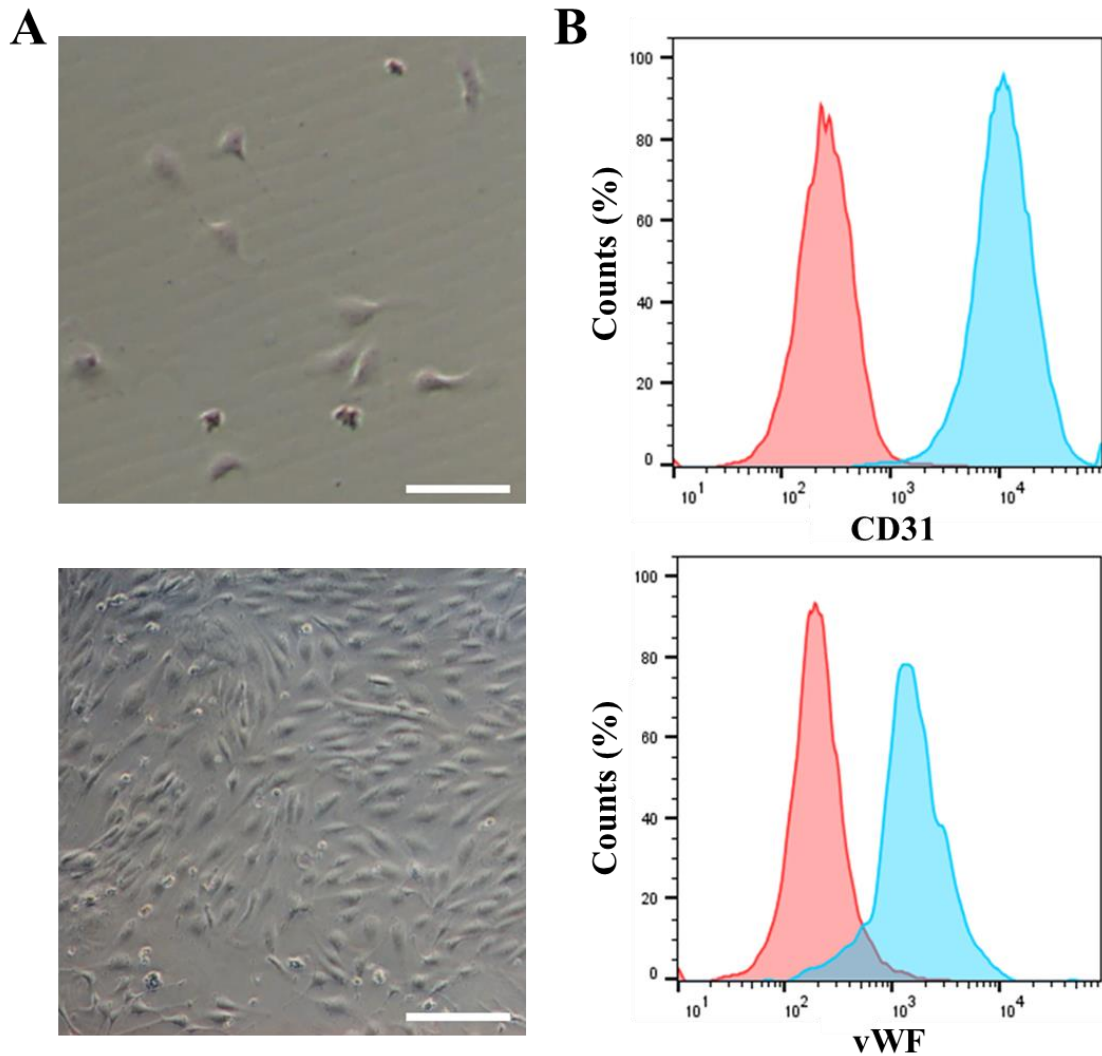
Figure 4-6 Characterization of HUVECs. (A) Cell shape illustrated the typical cobblestone form associated with HUVECS at both low and high densities. Cells became tightly packed but did not overlap one another when maintained at confluence. The scale bar is 200 µm. (B) HUVEC purity was assessed by flow cytometry. CD31 (light-blue area) was detected in 99.5% of cells and vWF (light-blue area) was detected in >95% of cells compared with an isotype control (red areas).

4.2.2 Cell viability assay for HUVECs

Prior to evaluating the effects of varying stiffness of PEEU fiber meshes on the angiogenic potential of HUVECs, we first determined whether the cells could survive on PEEU fiber mesh scaffolds. All four types of PEEU fiber meshes were explored in the biological studies. Immunofluorescence staining was carried out on HUVECs cultured on PEEU fiber meshes, and both living and dead cells could be detected, as shown in Figure 4-7 (A). The result showed that the distributions of live and dead cells were similar for cultured grown on all four types of

PEEU fiber mesh scaffolds. Living cells accounted for greater than 80% of the detected HUVECs cultured on all four types of PEEU fiber meshes scaffolds (Figure 4-7B). In contrast, only 63% of living HUVECs cells were observed on PDC scaffolds with randomly orientated fibers, reported by C. Ruder in [107]. Overall, large cell numbers and high percentages of viable cells were identified on all four types of PEEU fiber mesh scaffolds, which displayed relatively similar patterns of distribution, indicating that these electrospun PEEU fiber mesh scaffolds were relatively biocompatible and could be used for the culturing of HUVECs.
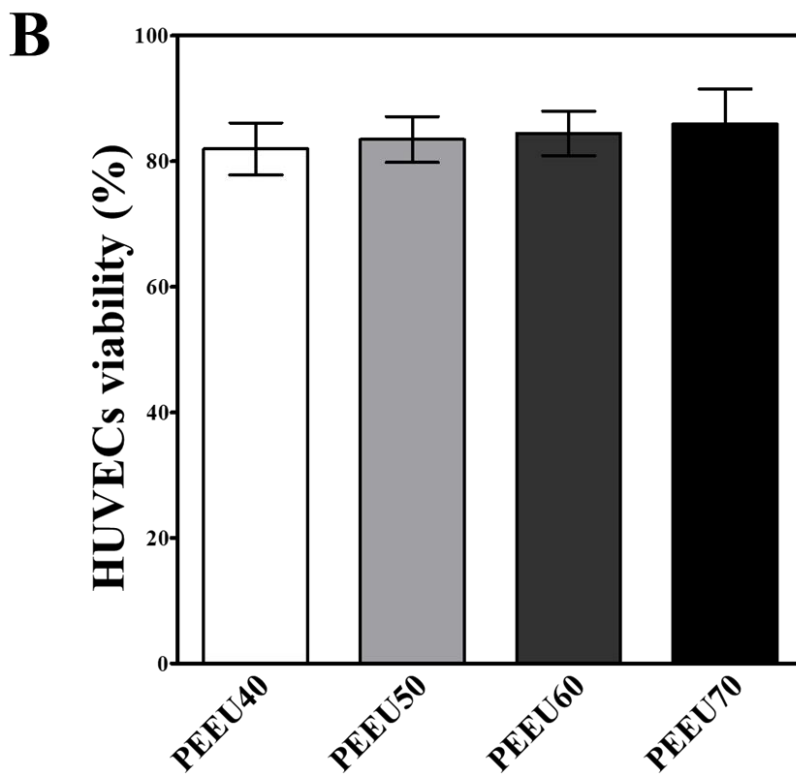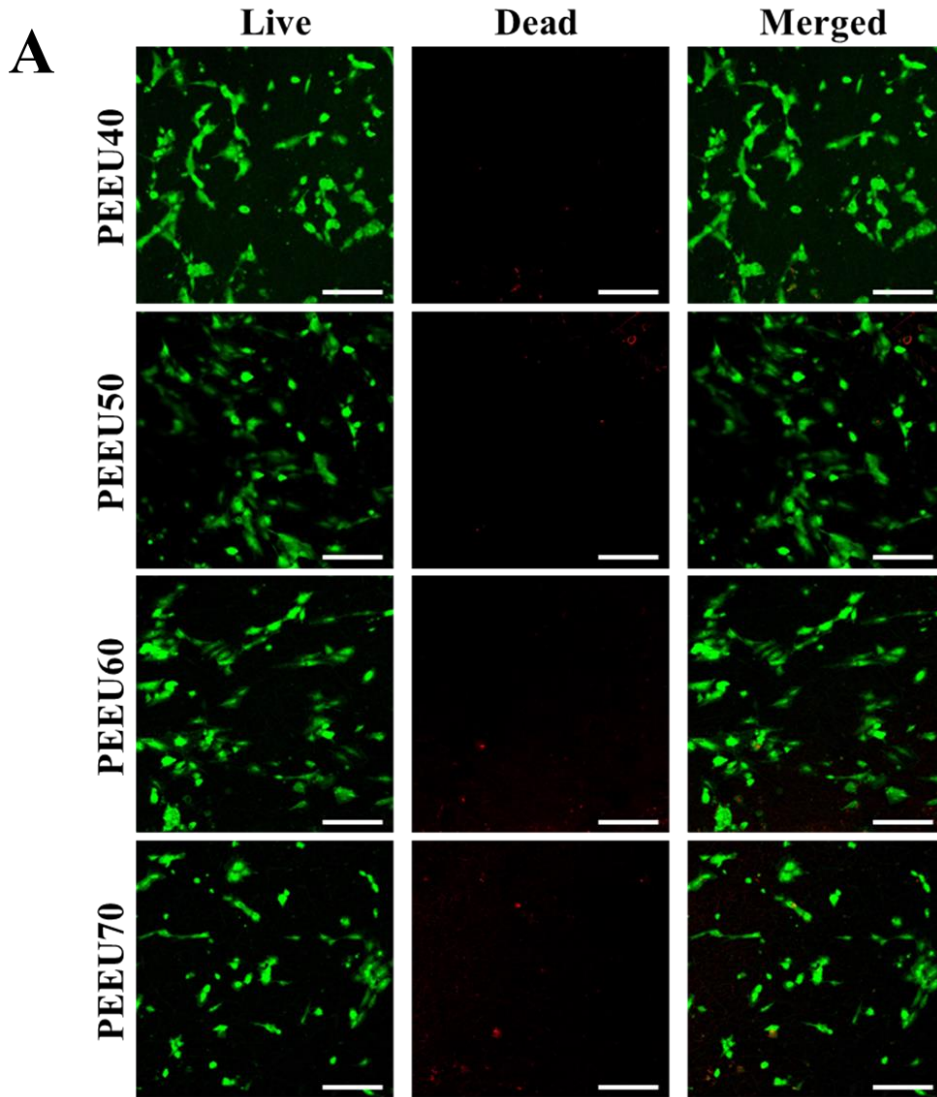
Figure 4-7 Cell viability assay performed in HUVECs cultivated on PEEU fiber meshes. (A) Fluorescence staining was taken to identify live and dead HUVECs cultured on fiber meshes derived from all PEEU scaffolds after 6 days of culture. Calcine acetomethoxy (AM; green) was used to label live cells, whereas ethidium homodimer (EthD)-1 was used to mark dead cells (red). The scale bar is 200 µm (B) HUVEC viability was calculated for different PEEU scaffolds, the account of randomly selected graphs used for analysis was: (n $_{PEEU40}$ = 6; n $_{PEEU50}$ = 6; n $_{PEEU60}$ = 6; n $_{PEEU70}$ = 6). There is the same cell viability among all four PEEU scaffolds. The data was statistically analyzed by one-way ANOVA result with Tukey's test of multiple comparisons. $p < 0.05$, *. The data is presented as mean ± SD.

4.2.3 Cell morphology analysis of HUVECs

The morphologies of HUVECs cultivated on various PEEU fiber meshes were stained and imaged by a confocal laser scanning microscope. Merged fluorescent images showing actin cytoskeleton and nuclear staining in HUVECs are shown in Figure 4-8 (A). The imaging results indicated that HUVECs were able to attach well to the various PEEU fiber meshes while presenting various morphologies. The cells cultivated on the soft fiber meshes, such as PEEU40 and PEEU50, showed a flat appearance, whereas on the relatively stiff PEEU60 and PEEU70 scaffolds, the cells displayed elongated shape, with a higher aspect ratio, as shown in Figure 4-8 (B). These results were consistent with those of previously published reports, in which HUVECs demonstrated more rounded shapes on softer materials and more elongated shapes on stiffer materials [68].

A

B
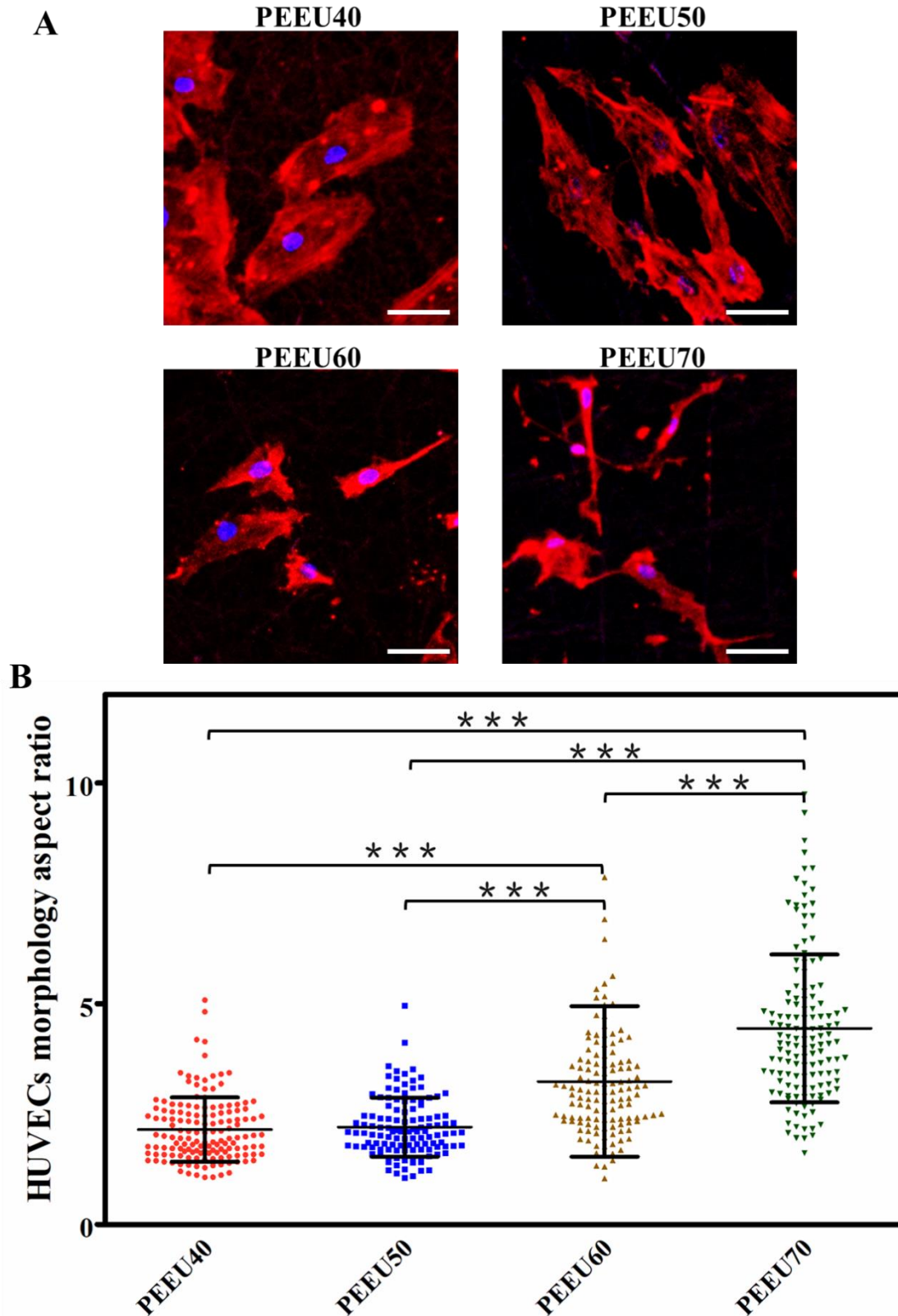
Figure 4-8 Morphologies of HUVECs cultivated on different PEEU fiber meshes scaffolds. (A) Cell nuclei were dyed blue, whereas F-actin was stained red. (B) The distributions of the HUVEC morphology aspect ratios were shown, (n > 200). One-way ANOVA with Tukey's

multiple comparisons test was used to statistically evaluate the data. $p < 0.001$, ***. The data is shown as mean $\pm$ SD. The scale bar is 50 µm.

4.2.4 HUVEC proliferation assay

The proliferation of HUVECs cultured on the various PEEU scaffolds was measured by a cell counting kit 8 assay. The HUVEC proliferation results for the various PEEU fiber meshes materials are presented in Figure 4-9. The densities of cells cultured on the all-prepared scaffolds increased with a longer incubation time, and a high density of adhering cells on the scaffolds was reached with no significant difference among different PEEU scaffolds after 9 days culture showed a good proliferation potential of HUVECs on all PEEU scaffolds. On day 1, The initial number of cells attached to PEEU40 and PEEU70 fiber meshes were similar with no significant differences identified. Also, there were no difference between PEEU50 and PEEU60 in cell number. Significant differences in cell numbers were observed between PEEU40 and PEEU70 scaffolds on the third day of the incubation. On day 6, significant differences in HUVEC proliferation were detected among PEEU scaffolds become visible, with a significantly increased number of HUVECs cultured on the PEEU70 fiber mesh scaffold compared with the number of HUVECs cultured on the PEEU40. A larger number of HUVECs was also observed on the PEEU60 fiber mesh scaffold compared with the numbers of cells cultured on PEEU50 with significant difference. Also, cells number of HUVECs on the PEEU60 fiber mesh scaffold was higher than that on PEEU40, but this difference showed no significant difference.

These results demonstrated that cell growth occurred at a faster rate on the more elastic PEEU fiber mesh scaffolds compared with the less elastic scaffolds, which suggested that scaffolds with increased elasticity could promote HUVEC growth.

The results was in line with the findings of a previously published article, which found that substrate stiffness affects EC proliferation through regulating the activation of the SEPT9-Src-Vav2-Rho A pathway [9]. In addition, substrates characterized by high stiffness can induce the nuclear translocation of the transcription factors yes-associated protein (YAP) and TAZ, which can stimulate the expression of a large number of downstream target genes, promoting cell growth, migration, and angiogenic potential [110-112].
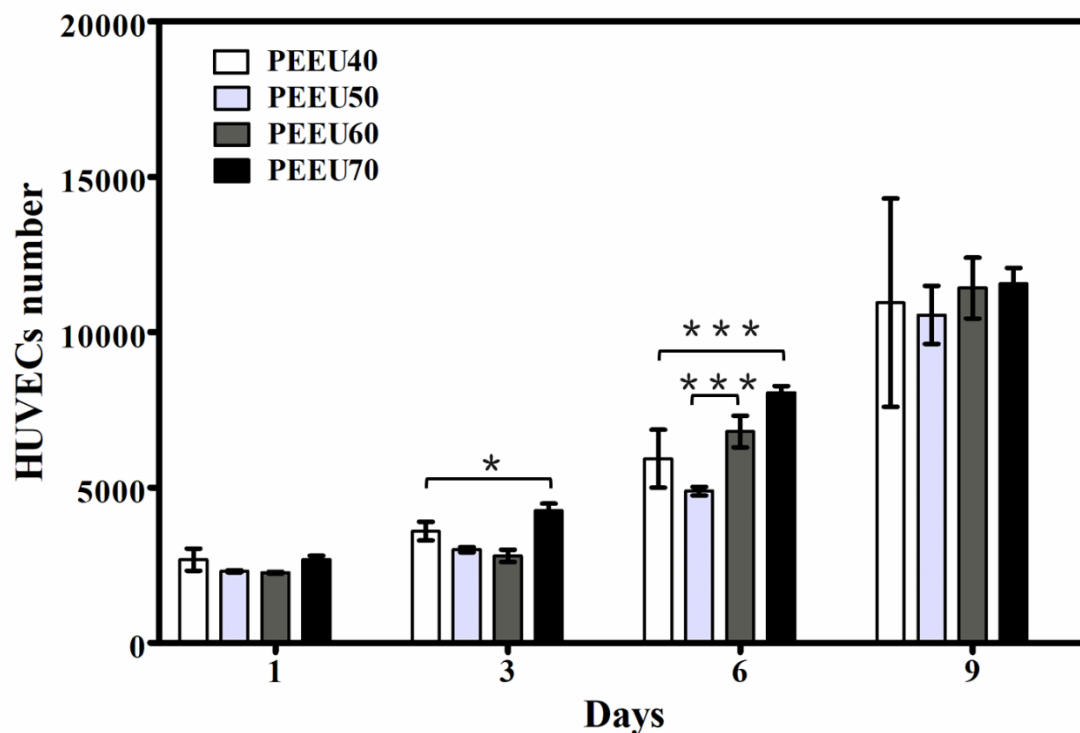
Figure 4-9 HUVEC proliferation rates cultured for different lengths of time on different PEEU fiber meshes. The data was statistically examined by one-way ANOVA together with Tukey's multiple comparisons tests. $p < 0.05$, *; $p < 0.001$, ***; n = 10. The data is shown as mean ± SD.

4.2.5 HUVEC migration

In addition to chemical and biological cues, the elasticity of the fiber meshes on which cells are cultured can also play an important role in the modulation of cell migration. The migration trajectories and velocities of HUVECs collected from PEEU40 and PEEU70 fiber mesh scaffolds are shown in Figure 4-10. The average migration velocities of cells harvested from fiber mesh scaffolds formed using PEEU40 materials and those from fiber mesh scaffolds formed using of PEEU70 were 0.058 ± 0.019 and 0.076 ± 0.018 µm/min, respectively, which represented a significant difference. These results showed that cells cultivated on the stiffer fiber mesh scaffold derived from PEEU70 exhibited a quicker migration rate than cells cultivated on the PEEU40 fiber meshes scaffold with a lower elasticity. This result was consistent with previous studies [58], and is likely due to the cell sensing and responding to fiber meshes stiffness through integrin-binding and the resulting traction forces exerted by integrin cytoskeleton interactions [113]. The stiffer materials is thought to contribute to a stronger contractile force, inducing increased movement by the cells.

A

B
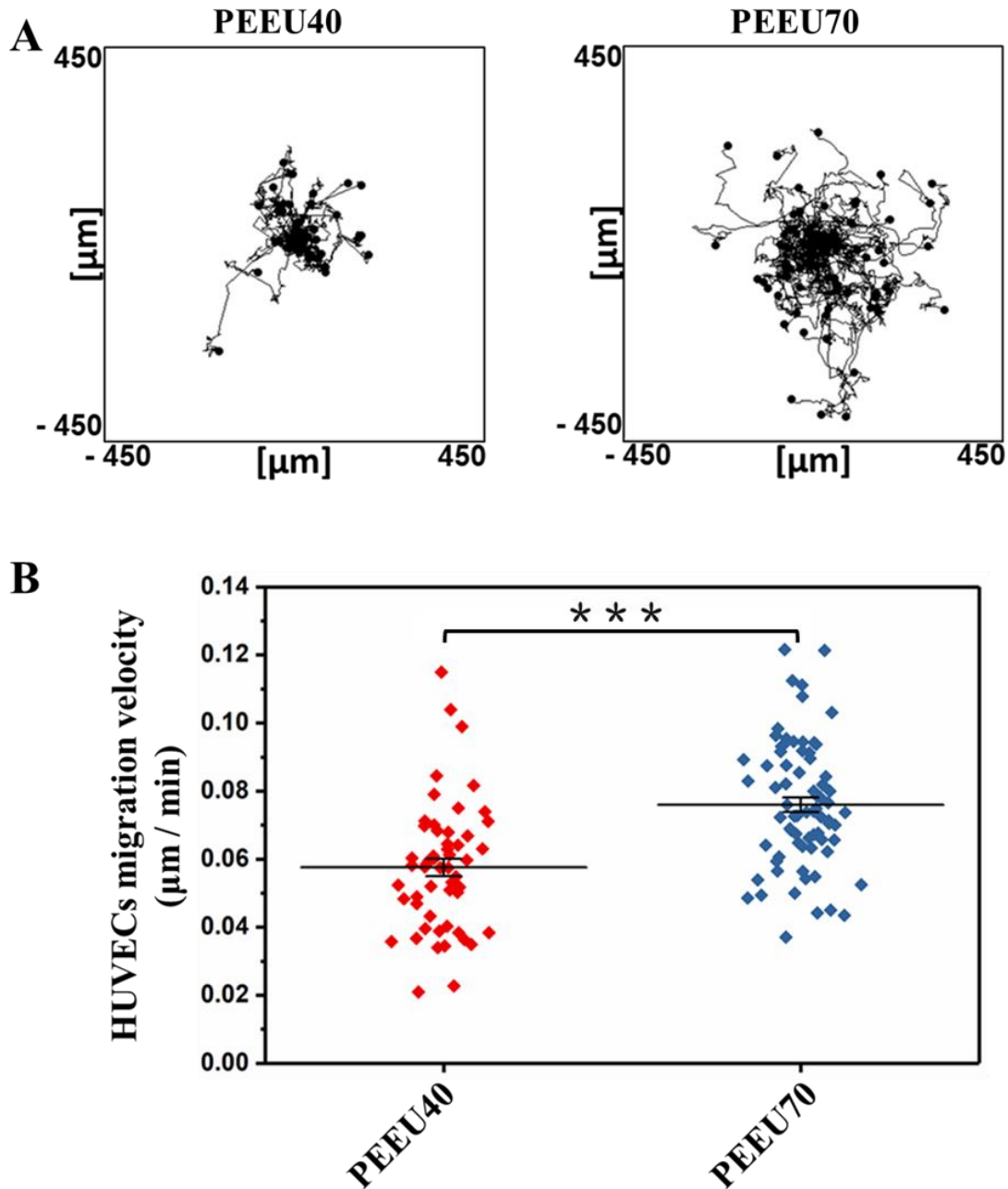
Figure 4-10 HUVEC migratory results for cells cultivated on PEEU40 and PEEU70 fiber meshes. (A) A time-lapse microscope was used to capture the cell migratory trajectories, which were then analyzed by Image J software. (B) The HUVEC velocities were shown (n $_{PEEU40}$ = 54; n $_{PEEU70}$ = 74). Student's t-test was used to statistically assess the data. $p < 0.05$, *. Results are presented as mean ± SD.

4.2.6 Analysis of HUVEC tube formation

The enhancement of EC growth and migration improves the capacity of ECs to self-assemble into tube like network structures [114]. Angiogenesis is the process of generating new blood vessels from existing ones, which is necessary for growth and development, wound healing, and the formation of tumors under pathological conditions. A widely used assessment of *in vitro* angiogenesis capabilities is the tube formation assay, which measures the ability of ECs to form 3D tube-like structures (capillary-like structures). The tube formation [79, 115] assay is a fast, sensitive, and quantifiable method for *in vitro* measurement of angiogenesis and thus can be applied to high throughput screening to identify which factors potentially promote or restrain angiogenesis [116].

PEEU40 and PEEU70 fiber meshes were used to study how changes in substrate stiffness affect the angiogenesis capacity of HUVECs, using the tube formation assay. Photos of a tube formation test with capillary like tube formations, are displayed in Figure 4-11 (A), and the data analysis results are displayed in Figure 4-11 (B and C). Prominent capillary-like networks with a increased number of branching points and longer capillary tube lengths were observed in HUVECs harvested from the PEEU70 fiber mesh scaffolds, which generated a greater number of closed loops (about 13.6 ± 5.6 per square millimeter), whereas HUVECs collected from PEEU40 fiber meshes formed 7.3 ± 2.4 totally closed tubes per square millimeter. The total lengths of tubes were approximately 10,000 ± 1,500 µm and 11,500 ± 1,000 µm per field of view in cells collected from PEEU40 and PEEU70 fiber meshes scaffolds, respectively.

The tube formation results revealed that a significantly larger number of closed tubes and a significantly much longer total tube length was formed by the cells harvested from the PEEU70 fiber mesh compared with those formed by cells harvested from the PEEU40 fiber mesh. This is likely because stiffer fiber meshes can promote YAP nuclear translocation, which triggers the activation of multiple downstream target genes, and subsequently promotes angiogenesis [110-112]. The results indicated that compared with the PEEU40 substrate, the PEEU70 substrate appears to possess an increased proangiogenic potential for the induction of increased EC differentiation.
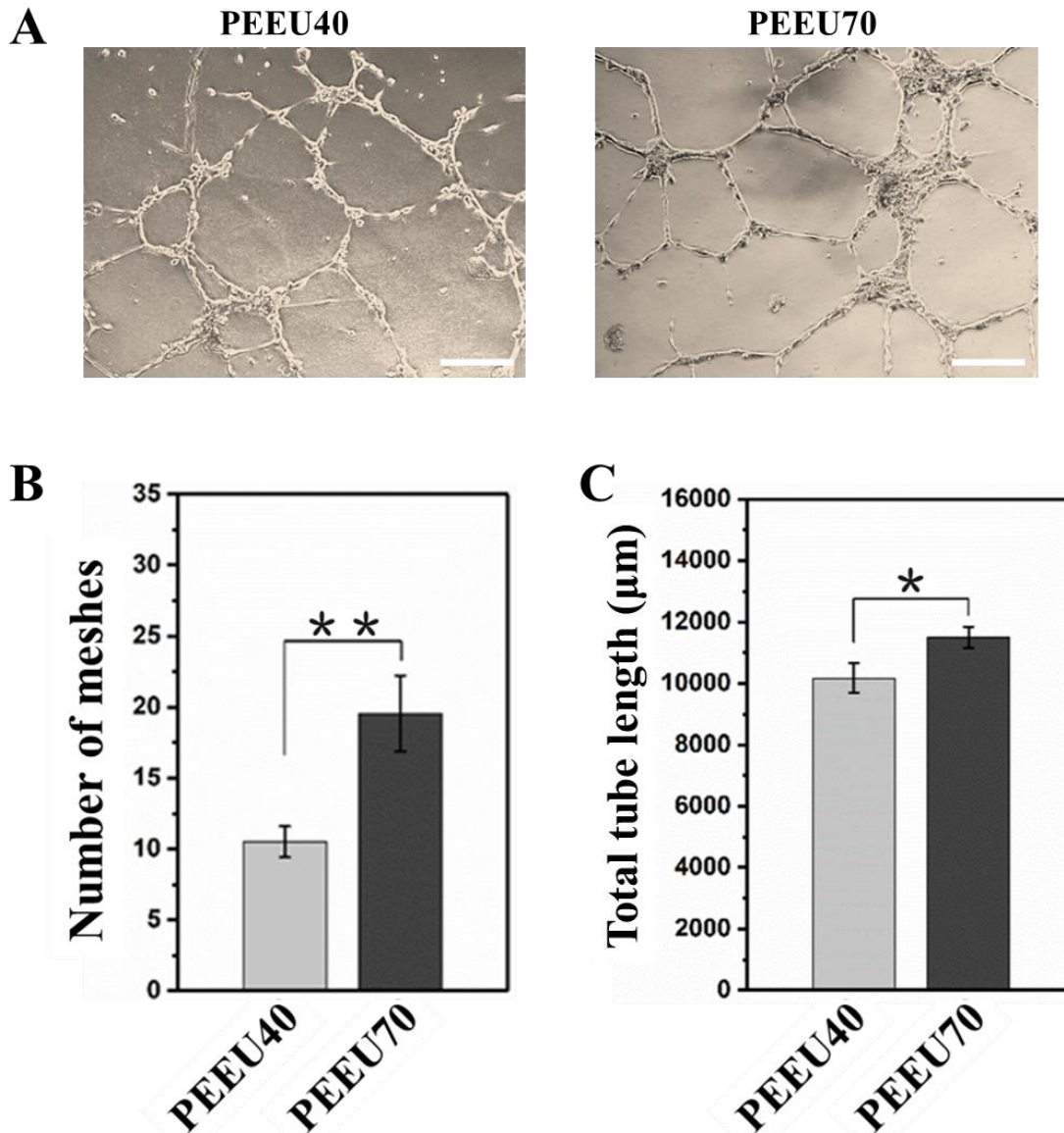
Figure 4-11 Tube formation assay of HUVEC. (A) Images showing the tube formation results of HUVECs cultivated on PEEU40 and PEEU70 fiber meshes. The scale bar is 200 µm. (B) The formation of closed tubes of HUVECs were numbered, and (C) the overall tube length was calculated in the acquired photos. (n $_{PEEU40}$ = 9; n $_{PEEU70}$ = 10). Student's t-test was used to statistically assess the data. $p < 0.05$, *. Results are expressed as mean ± SD.

4.3 Effects of electrospun fiber meshes stiffness on hADSC osteogenic differentiation

Stem cells are strongly influenced by their environmental niches, and alterations in this microenvironment have the potential to dramatically modify cell behaviors and differentiation

capacities. This section describes studies performed to examine difference in hADSC viability, morphology, nuclear shape, and osteogenic differentiation when hADSCs are grown on fiber meshes derived from various PEEUs, which feature different stiffness characteristics.

4.3.1 hADSC viability assay

Prior to evaluating the effects of different stiffness of PEEU fiber mesh on the osteogenesis of hADSCs, the ability of these cells to survive on PEEU fiber mesh scaffolds for the duration of the culture period was assessed. All four types of PEEU fiber mesh scaffolds were tested in these biological studies. Immunofluorescence cell viability staining revealed that the cell distributions were similar on all four types of PEEU fiber mesh scaffolds (Figure 4-12). Over 90% viability of hADSCs cultured on all four types of PEEU fiber mesh scaffolds. These results indicated that the PEEU fiber mesh scaffolds prepared by the electrospinning method were relatively biocompatible and could be used to culture hADSCs.
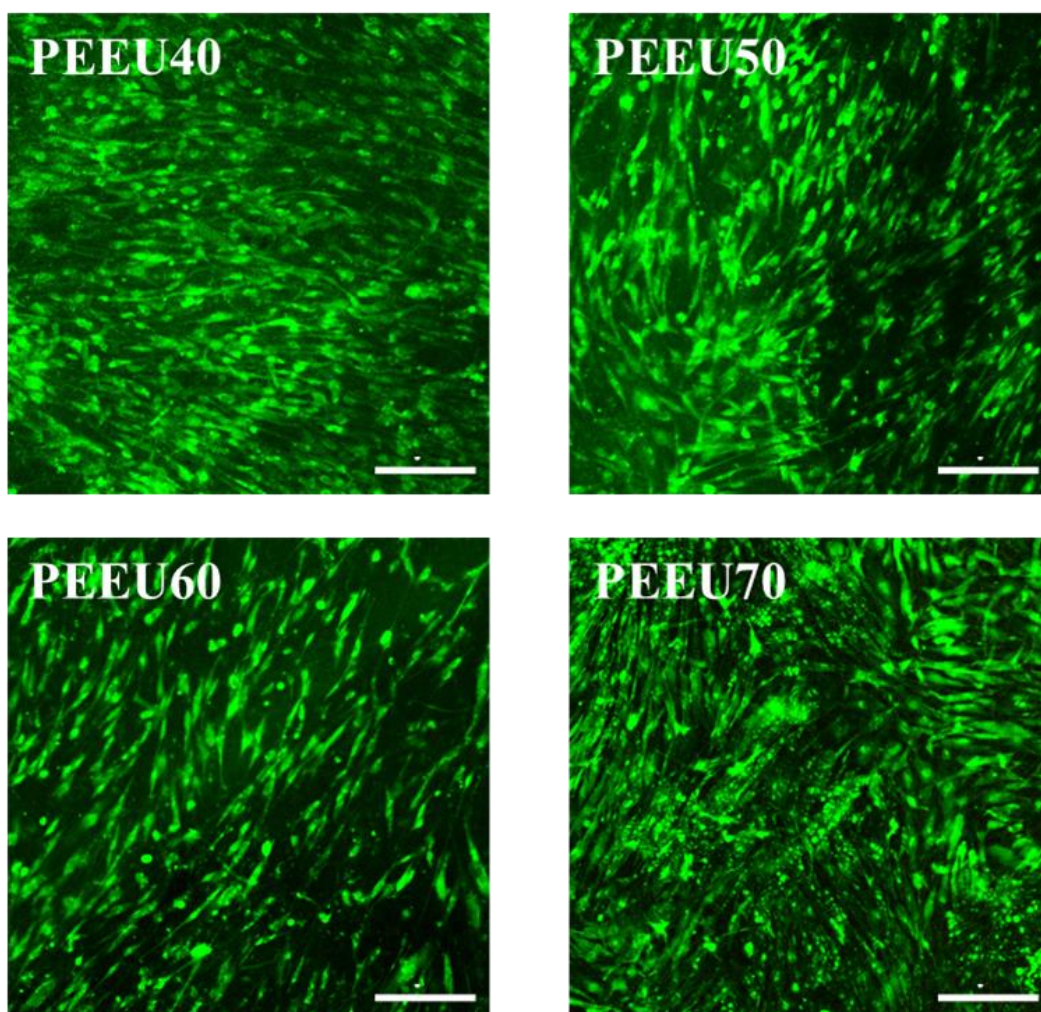
Figure 4-12 Images of hADSCs viability after being cultured on different PEEU fiber meshes for 6 days incubation in growth medium. Calcine acetomethoxy (AM; green) was used to label live cells, whereas ethidium homodimer (EthD)-1 was used to dye dead cells (red). The scale bar is 200 µm.

4.3.2 Cell morphology analysis of hADSCs

hADSCs are capable of differentiating into multiple lineages, a process that is regulated by many factors in the ECM. Several research have indicated that cell shape plays an important function in determining whether hADSCs commit to an adipocyte or osteoblast lineage. In addition, studies have shown that adhered, flattened, and extended hMSCs typically prefer osteogenesis, whereas more round cells typically underwent adipogenesis [20].

Previous studies have shown that cells could be modulated by changes in the ECM elasticity [117]. Therefore, the attachment and morphologies of hADSCs cultured on PEEU fiber mesh scaffolds with different elasticities were studied. Merged fluorescent images in which the actin cytoskeleton and nuclei of hADSCs were stained are shown in Figure 4-13 (A). The polarized morphologies of cell bodies grown on different PEEU scaffolds were assessed by quantifying the aspect ratio of the cell body. The results showed that hADSCs were capable of attaching well to all of the prepared PEEU fiber mesh scaffolds, although they presented with different morphologies on different scaffolds. These findings revealed that the various PEEU fiber meshes stiffness were able to modulate hADSC morphologies. The cells exhibited a shorter aspect ratio on the soft fiber meshes (such as PEEU40 and PEEU50), whereas, on the stiffer PEEU60 and PEEU70 scaffolds, the cells presented larger aspect ratios as shown in Figure 4-13 (B). As shown by the quantitative data, as the matrix stiffness increased, the cell aspect ratio also increased. The data is in agreement with previously published findings [117], and the elongated cell morphologies observed on stiffer materials could be attributed to the increased formation and organization of the F-actin cytoskeleton [118]. The results implyed that the application of stiffer PEEU fibers mesh scaffolds as a culture substrate contributed to the elongation of hADSC morphology and might promote osteogenic differentiation.
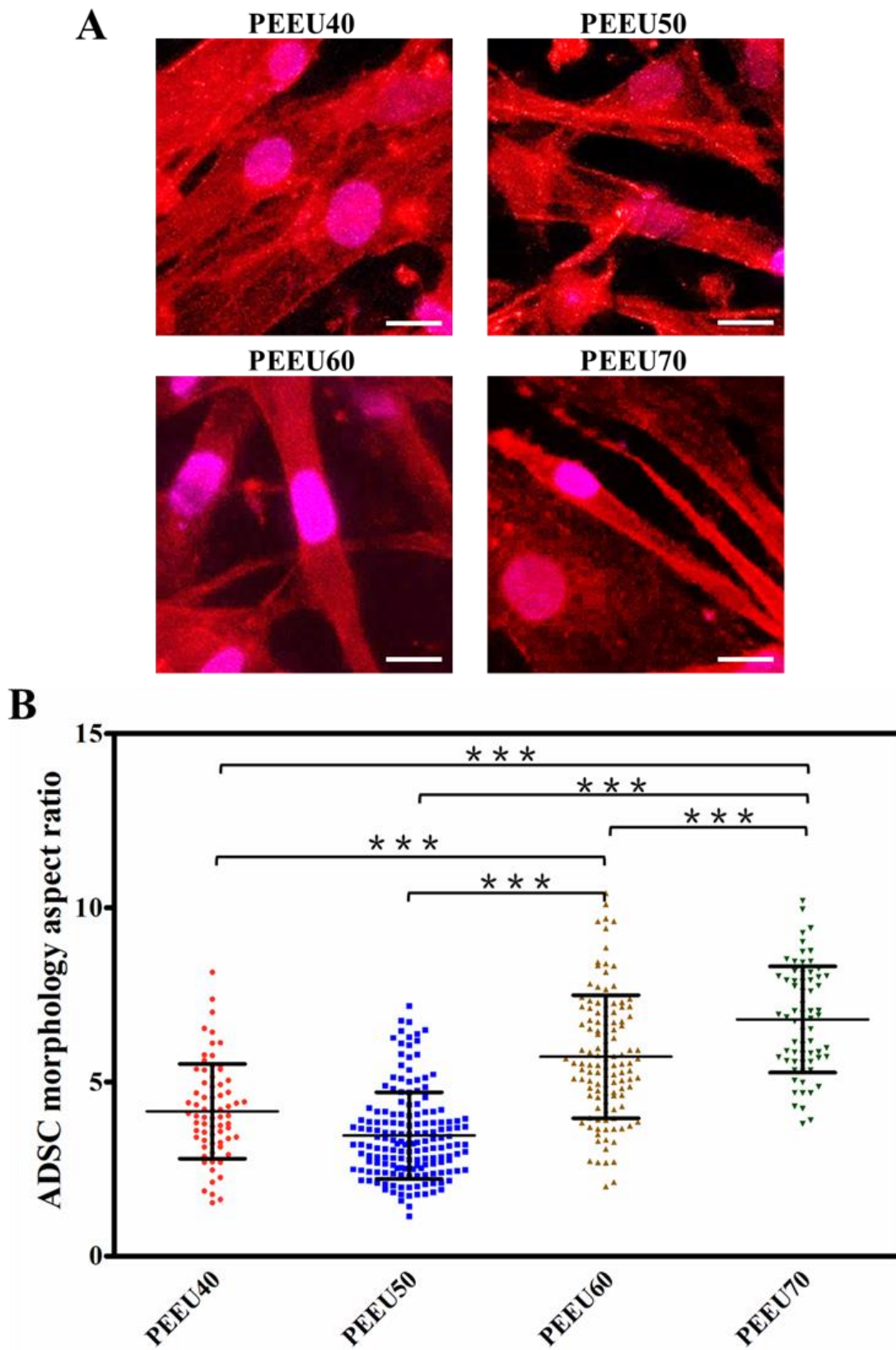
Figure 4-13 Changes in the cell morphology of hADSCs grown on fiber mesh substrates with different stiffness characteristics. (A) Fluorescent images showing the morphologies of cells cultured on PEEU40, PEEU50, PEEU60, and PEEU70 fiber mesh scaffolds. Cell nuclei were

dyed blue, whereas F-actin was stained red. The scale bar is 20 μm. (B) Cell aspect ratio measured in hADSCs cultured on different fiber mesh scaffolds. The total number of cells that were counted of each group was >350. An increased of cell morphology aspect ratio was demonstrated with increasing fiber meshes stiffness, yet no statistically significant difference was found. The data was statistically analyzed using Tukey's multiple comparisons test together with one-way ANOVA. $p < 0.001$, ***. The data is shown as mean ± SD.

4.3.3 Measurement of hADSC nuclear shape

The results of the previously described experiments indicated that differences in the stiffness of these PEEU fiber mesh scaffolds were associated with significant differences in the shapes of hADSCs cultured on these scaffolds. We investigated whether the range of elasticity exhibited by our prepared PEEU fiber meshes was also associated with changes in the shape of the cell nuclei. Fluorescent images of hADSC nuclei can be observed in Figure 4-14 (A). The nuclei of hADSCs were longer on stiffer PEEU fiber mesh scaffolds, and shorter on softer PEEU fiber mesh scaffolds. In addition, the nuclei appeared more rounded in hADSCs cultured on low elasticity PEEU fiber mesh scaffolds, whereas those grown on high elasticity PEEU fiber mesh scaffolds, featured elongated nuclei with expanded shape. Figure 4-14 (B) presents the quantification of the nuclear aspect ratios and nuclear sizes from at least 170 cells grown on each substrate. A clear increase in the nuclear aspect ratio can be observed when comparing the soft substrates against the stiff substrates. The nuclear aspect ratios of cells grown on fiber mesh scaffolds derived from PEEU40, PEEU50, PEEU60, and PEEU70 materials were 1.5 ± 0.2, 1.5 ± 0.3, 1.6 ± 0.4, and 1.5 ± 0.3, respectively. The nuclear aspect ratios measured in cells grown on the stiffer PEEU60 and PEEU70 scaffolds were significantly higher than those measured in cells cultured on the softer PEEU40 and PEEU50 scaffolds. These results are consistent with those of a previously reported study, in which the rigidity of a cell substrate was shown to control changes in the nuclear shape [24, 119-121]. Changes in the nuclear shape can modulate alterations in the structure and organization of chromatin, which can, in turn, modulate the transcription procedure and, consequently, alter the differentiation processes of stem cell [20]. These results indicated that the elasticity of the PEEU fiber meshes can potentially alter the shape of nuclei, similar to the observed effect of mechanical ECM stimulation, which can be transferred from the cell-substrate interface to the

cell nuclei to alter cellular functions.
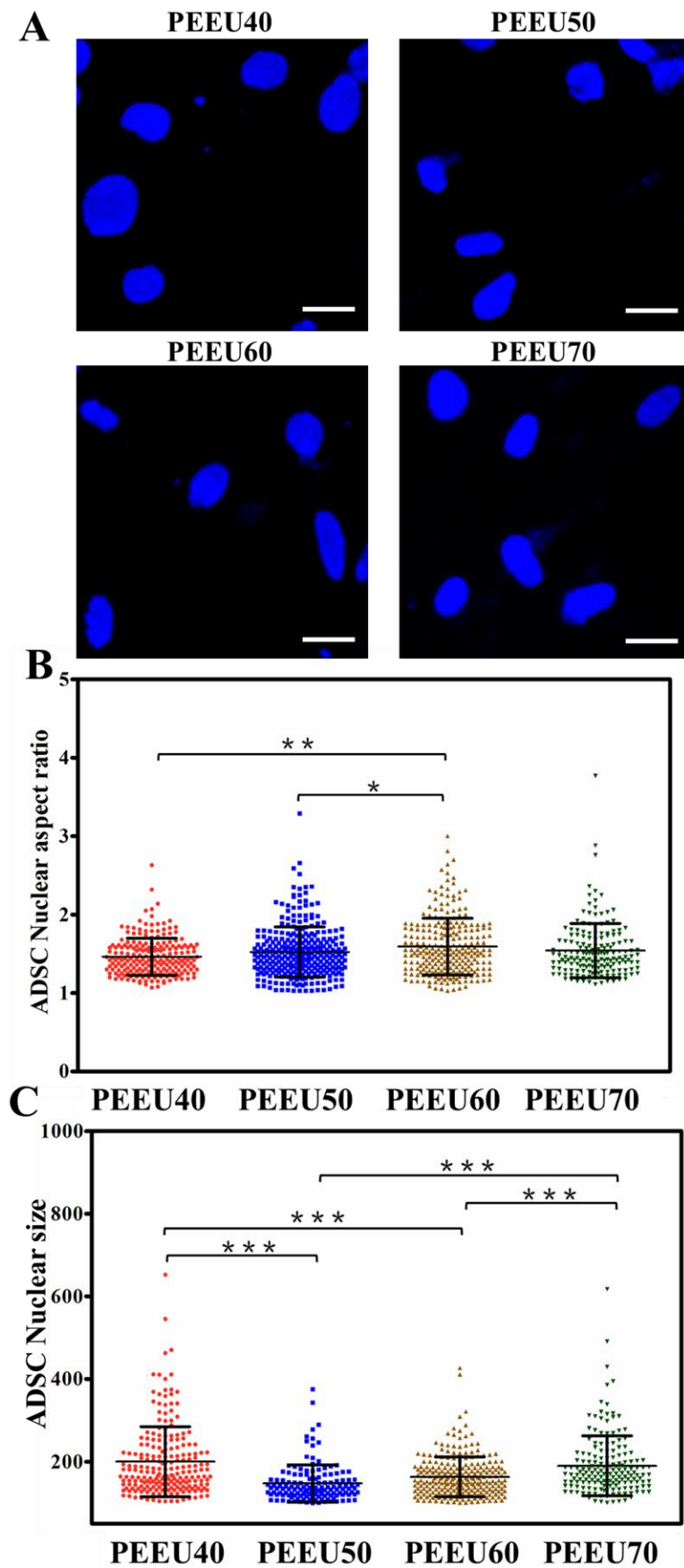
Figure 4-14 The nuclear shape of hADSCs depends on the stiffness of the PEEU fiber mesh scaffolds. (A) Fluorescent images of hADSCs cultured on different PEEU fiber meshes and stained for nuclei (blue). Nuclei become more elongated with the increased stiffness of the PEEU fiber mesh scaffolds. The scale bar is 20 μm. (B) Graphical representation of the hADSCs nuclear aspect ratios measured in cells cultivated on the all types of PEEU fiber mesh scaffolds. (C) hADSCs grown on various PEEU fiber mesh scaffolds have significantly different nuclear sizes. The number of cells of each group counted was >170. One-way ANOVA together with Tukey's multiple comparisons test was used to statistically evaluate the data. $p < 0.05$, *; $p < 0.01$, **; $p < 0.001$, ***. The data is expressed as mean ± SD.

4.3.4 The high density of hADSCs cultivated on PEEU fiber meshes

Cell density can also regulate MSC differentiation [122, 123]. Whether hMSCs differentiate into adipocytes or osteoblast can be regulated by cell density. Low-density hMSCs prefer osteogenesis, whereas cells cultured at high densities have the high potential to become adipocytes [124].

The effects of cell density should be removed while investigating the impact of fiber mesh stiffness on osteogenesis in hADSCs. A high initial seeding density (1×10^5 cells/ cm^2) was used to achieve a similar high hADSCs density on all PEEU scaffolds. After cell attachment was achieved, F-actin and cell nuclei staining were used to assess cell densities on fiber meshes. Fluorescent images of hADSCs cultivated on various PEEU fiber mesh scaffolds are shown in Figure 4-15 (A). The results showed that hADSCs attached well to all scaffolds, with high confluence. The quantitative data showed that no significant differences in the cell confluence among the cells cultured on the different fiber mesh scaffolds (Figure 4-15 (B). Therefore, all differentiation experiments were performed starting at a similar cell density on all PEEU scaffolds.

A

B
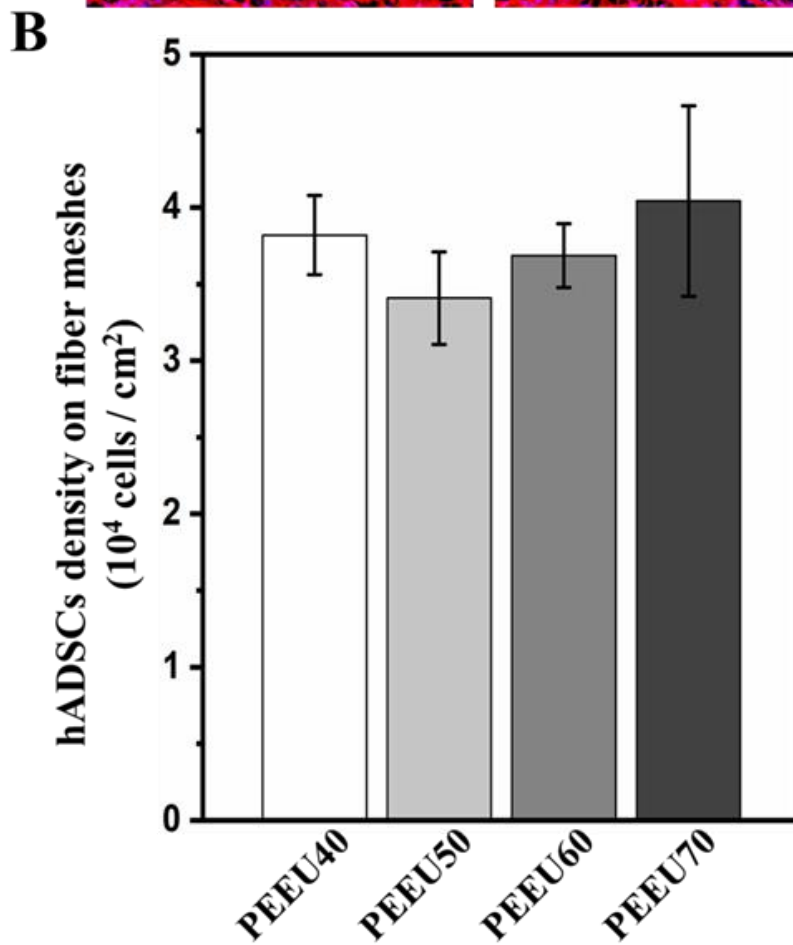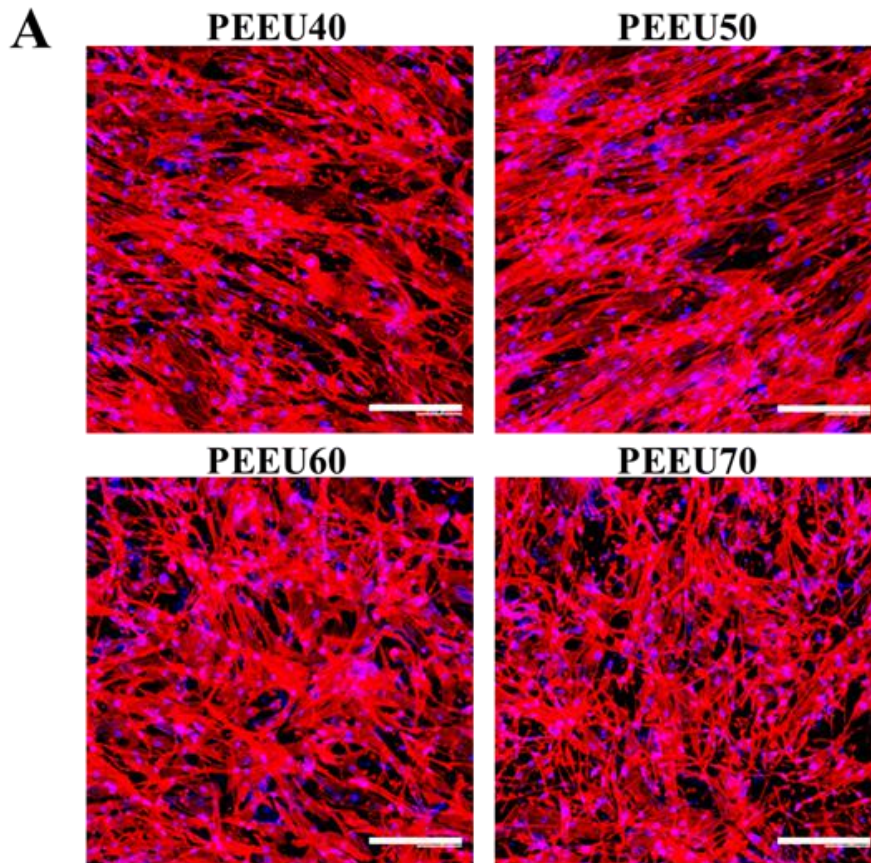
Figure 4-15 hADSC densities on fiber mesh scaffolds. (A) Merged fluorescent images of hADSCs cultured on all types of PEEU fiber mesh scaffolds and the cells nuclei were stained blue and F-actin was dyed red. Cells were seeded on all of the fiber mesh scaffolds at a high density. The scale bar is 200 µm. (B) hADSC densities were measured in representative images. (n $_{PEEU40}$ = 4; n $_{PEEU50}$ = 3; n $_{PEEU60}$ = 4; n $_{PEEU70}$ = 4); The results were statistically evaluated by Tukey's multiple comparisons test together with one-way ANOVA. The data is illustrated as mean $\pm$ SD.

4.3.5 Osteogenic differentiation assay

ALP activity measurement of hADSCs

To assess the osteogenesis of hADSCs on different fiber meshes, the activity of bone-specific ALP was investigated. The results showed that cells cultivated on the PEEU70 fiber meshes had the highest ALP activity, which was markedly higher than those in the other groups (Figure 4-16). These findings revealed that, as compared to softer PEEU fiber meshes, the fiber meshes with a stiffer PEEU fiber meshes could effectively enhance the osteogenesis of hADSCs.
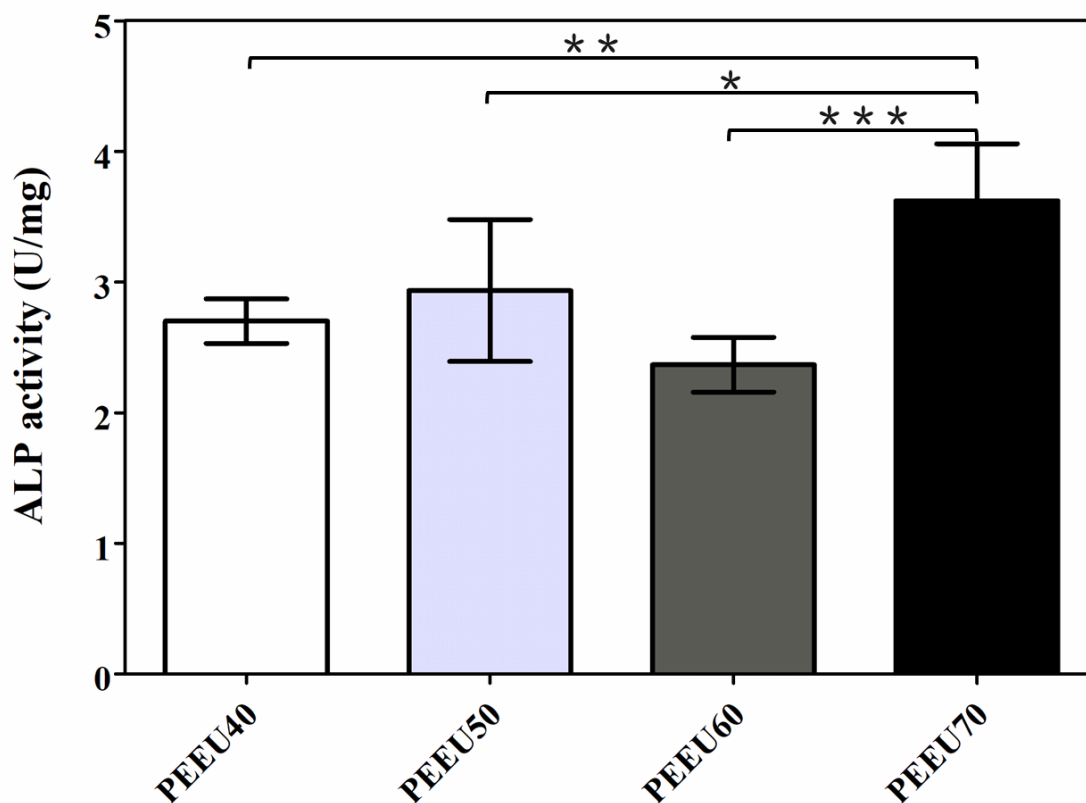
Figure 4-16 ALP activity levels were measured in cells cultivated on all types of PEEU fiber meshes. ALP activity was normalized to total protein levels. For quantitative analysis, at least four samples (n PEEU40 = 5; n PEEU50 = 5; n PEEU60 = 4; n PEEU70 = 6) were used. One-way ANOVA with Tukey's multiple comparisons test was used to statistically analyze the data. $p < 0.05$, *; $p < 0.01$, **; $p < 0.001$, ***. The data is represent as mean ± SD.

The osteocalcin expression quantification of hADSCs

The expression of the osteogenesis marker OCN in hADSCs cultivated on PEEU fiber meshes for three weeks in competitive differentiation media was measured using an enzyme-linked immunosorbent assay (ELISA) kit. A trend towards increased OCN levels was observed with increased fiber mesh stiffness (Figure 4-17). The OCN levels of cells cultured on the relatively stiffer fiber meshes (such as PEEU50, PEEU60, and PEEU70) were much higher than that in cells cultivated on the softer fiber mesh (PEEU40).
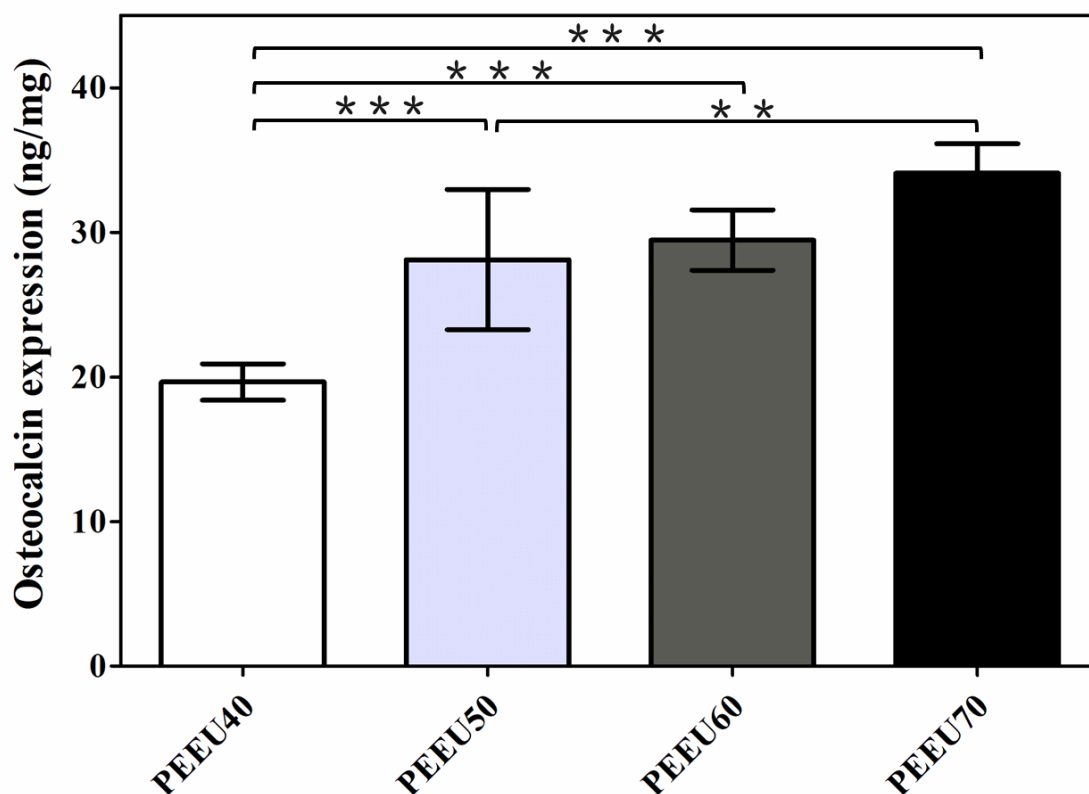
Figure 4-17 The levels of osteocalcin expression in hADSCs on various PEEU fiber meshes. The osteocalcin levels were quantified by ELISA. The results were normalized against total protein levels. Stiffer PEEU fiber meshes promotes the osteocalcin expression. Six samples of each group used for quantitative analysis. The data was statistically analyzed by one-way ANOVA with Tukey's multiple comparisons test. $p < 0.01$, **; $p < 0.001$, ***. The data is represented as mean ± SD.

RUNX2 nuclear translocation assessment in hADSCs

During differentiation processes, MSCs can give rise to several lineages, including myoblasts, osteoblasts, chondrocytes, and adipocytes [125]. MSC differentiation is primarily controlled by a group of proteins known as master transcriptional regulators [126]. Adipogenesis is regulated by peroxisome proliferator-activated receptor-gamma (PPARγ), whereas osteogenesis, is regulated by runt-related transcription factor 2 (RUNX2, also known as core-binding factor alpha 1, CBFα1). RUNX2 promotes the differentiation of MSCs into immature osteoblasts and stimulates the expression of key bone matrix genes during the early phases of osteoblast differentiation. RUNX2 is a transcription factor and exerts its role in the nucleus. To evaluate the nuclear translocation of RUNX2, cells were fixed and stained for RUNX2 after culturing on PEEU fiber mesh scaffolds for 21 days in 50% (v/v) adipogenesis-inducing media and 50% (v/v) osteogenesis-inducing media.

As shown in Figure 4-18, cells cultivated on PEEU70 fiber meshes displayed a higher RUNX2 nuclear translocation percentage compared with cells grown on PEEU40, PEEU50, and PEEU60 fiber mesh scaffolds. The percentages of RUNX2 nuclear translocation in cells grown on PEEU40, PEEU50, PEEU60, and PEEU70 fiber mesh scaffolds were $64.8 \pm 13.4\%$, $69.6 \pm 10.0\%$, $68.7 \pm 8.8\%$, and $89.9 \pm 3.5\%$, respectively. The percentage of nuclear-localized RUNX2 (Figure 4-19) in hADSCs cultivated on the PEEU70 scaffold was more higher than those in cells cultured on the other PEEU scaffolds, which indicated that hADSCs cultured on stiffer PEEU70 scaffolds preferably underwent osteogenic differentiation compared with hADSCs cultured on softer scaffolds (PEEU40, PEEU50, and PEEU60).
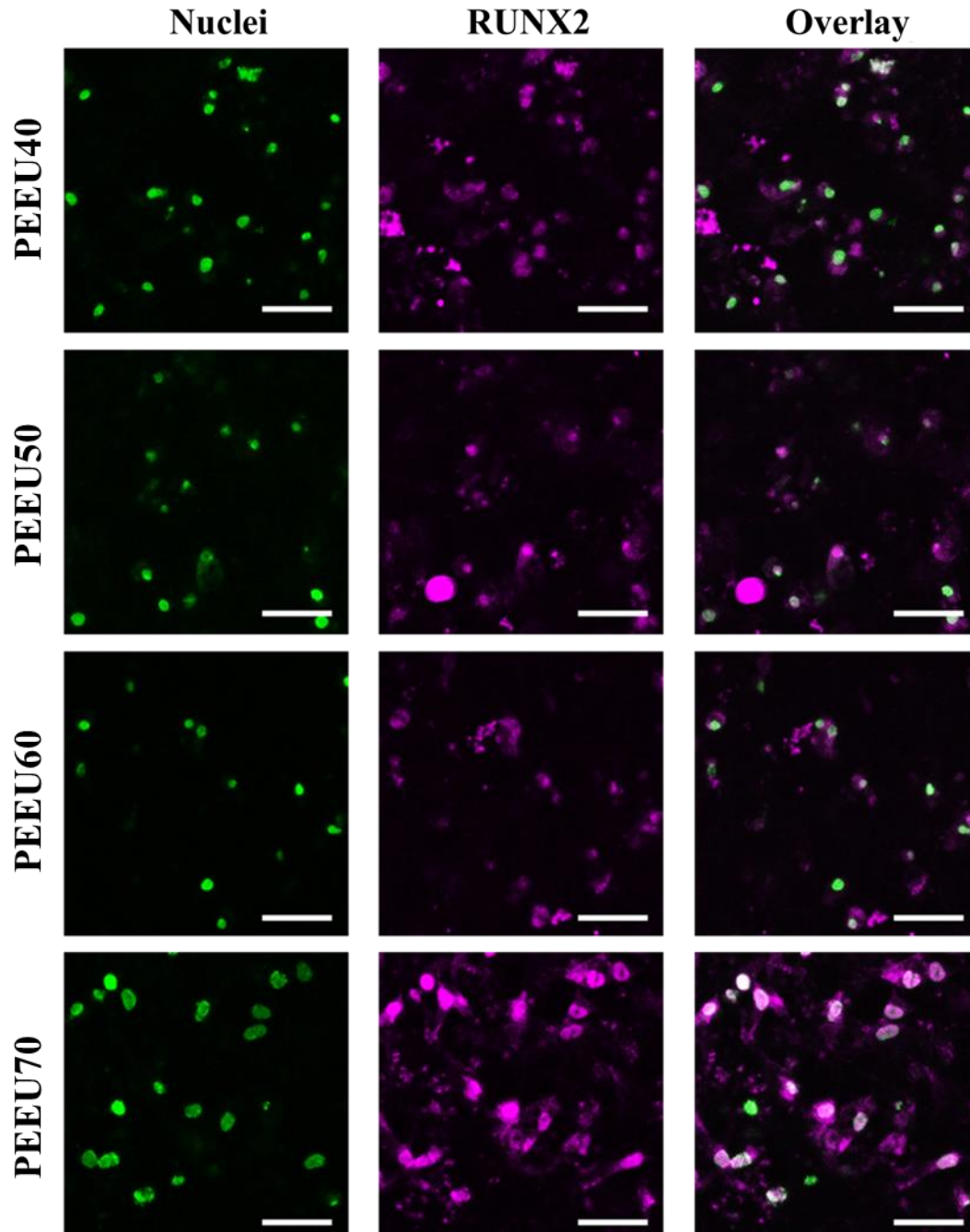
Figure 4-18 Images showing the immunofluorescent staining of RUNX2 expressed by hADSCs cultured on different PEEU fiber mesh derived from PEEU40, PEEU50, PEEU60, and PEEU70, characterized by different stiffness levels. hADSCs were stained for Nuclei (green) and RUNX2 (pink). Cells were grown in a mixed differentiation medium for three weeks. The scale bar is 50 μm.
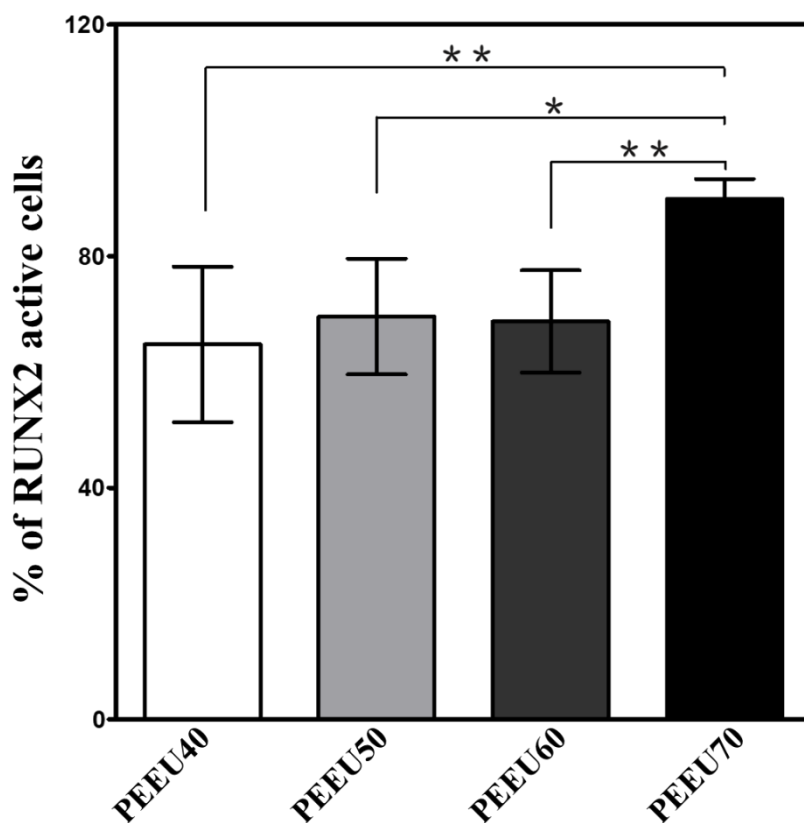
Figure 4-19 Analysis of the percentage of nuclear RUNX2-positive hADSCs in culture grown on different PEEU scaffolds. Cells were grown in mixed differentiation medium for three weeks. At least five randomly selected graphs containing more than 150 cells in each group were analyzed using Tukey's multiple comparisons test together with a one-way ANOVA. $p < 0.05$, *; $p < 0.01$, **. The data is shown as mean ± SD.

Osteoblast mineralization quantification of hADSCs

During osteogenic differentiation, cells remodel the surrounding ECM by producing ECM proteins and regulators of matrix mineralization. Mature osteoblasts can be characterized by the presence of a mineralized matrix due to the deposition of hydroxyapatite crystals [126].

To observe the expression of hydroxyapatite, cells were fixed and stained after culturing for 21 days in 50% (v/v) adipogenesis-inducing media plus 50% (v/v) osteogenesis-inducing media. As shown in Figure 4-20 (A), the fluorescence intensity of osteoblast mineralization (hydroxyapatite) of hADSCs was enhanced from fiber meshes scaffolds of PEEU40, PEEU50, PEEU60 to PEEU70. As shown in Figure 4-20 (B), the fluorescence intensities of hydroxyapatite normalized to total cell number, in cells cultured on PEEU40, PEEU50,

PEEU60, and PEEU70 fiber mesh scaffolds were $100.0 \pm 27.5\%$, $111.7 \pm 23.0\%$, $149.0 \pm 17.5\%$, and $157.9 \pm 45.8\%$, respectively. These data indicated that hydroxyapatite fluorescence intensity gradually increased from with increasing scaffold stiffness, with the lowest value observed for PEEU40, and the highest value observed for PEEU70. The fluorescence intensities were found to be significantly different among the PEEU40, PEEU60, and PEEU70 groups. The results indicated that as the elasticity of the PEEU fiber mesh scaffolds increased, the cells deposited an increasing quantity of hydroxyapatite in the ECM, which suggested that cells preferably underwent osteogenic differentiation when cultured on PEEU fiber mesh scaffolds with increased elasticity.
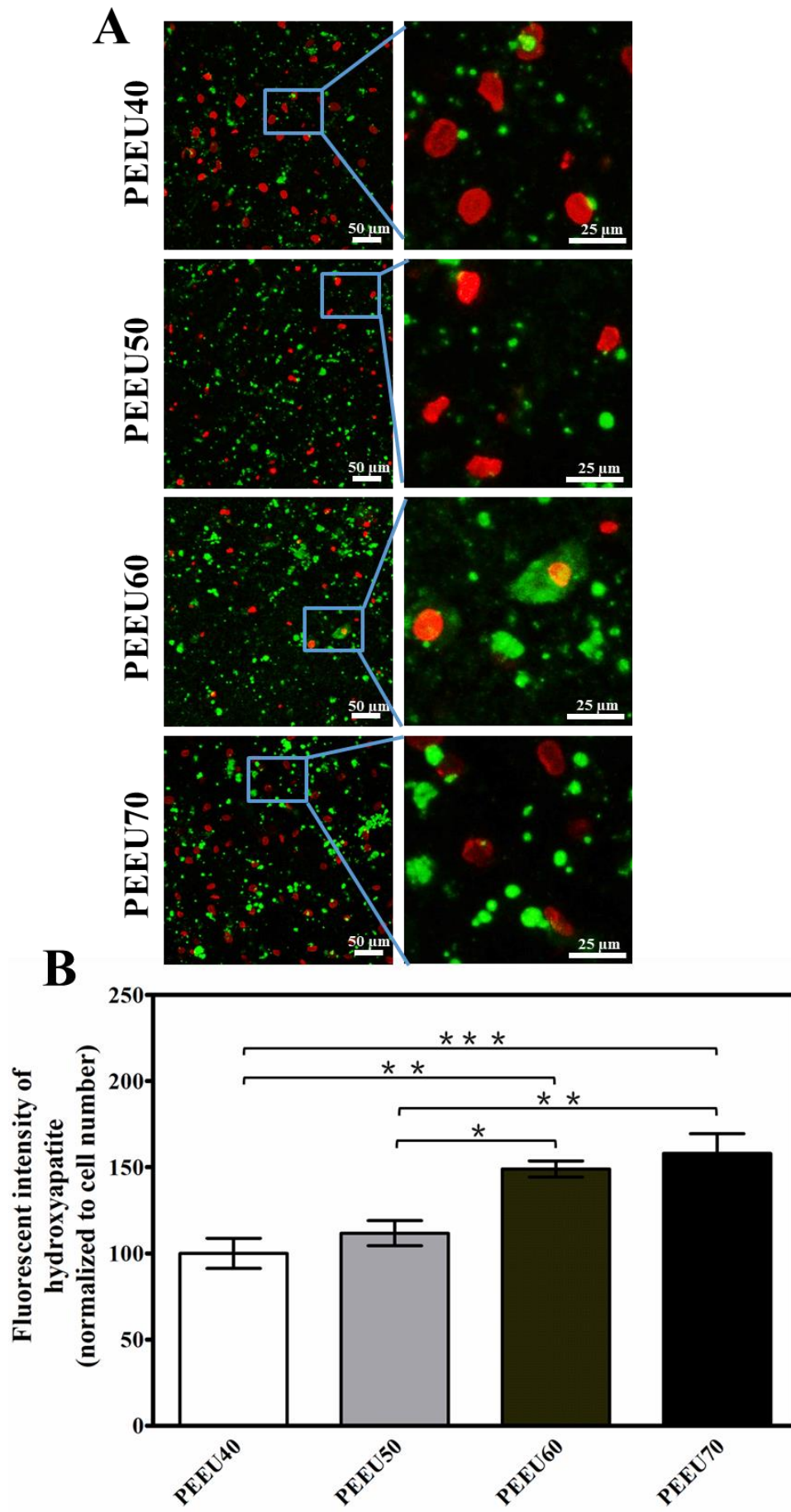
Figure 4-20 The influence of PEEU fiber mesh stiffness on hADSCs osteoblast mineralization. For three weeks, the cells were incubated in a mixed differentiation medium.. (A) Fluorescent images showing the osteoblast mineralization of hADSCs cultured on fiber mesh scaffolds derived from PEEU40, PEEU50, PEEU60, and PEEU70 and the cells' nuclei were stained red, whereas deposited hydroxyapatite were stained green. The fluorescence intensity of hydroxyapatite enhanced as a result of the increased stiffness of PEEU fiber meshes. The scale bar is 50 µm in the left row of pictures and 25 µm in the right row of pictures. (B) Quantification of hydroxyapatite fluorescence intensity, normalized by cell number, in cells seeded on various PEEU fiber meshes. At least ten randomly selected images of each group were used for quantitative analysis of osteoblast mineralization; the number of cells in these photos was calculated by counting the number of cells nuclei. Results were analyzed by Tukey's multiple comparisons test and a one-way ANOVA. $p < 0.05$, *; $p < 0.01$, **; $p < 0.001$, ***. Results are expressed as mean ± SD.

The observed preference of hADSCs cultured on stiffer scaffolds for osteogenic differentiation was consistent with previously reported findings, which showed that ECM stiffness regulates osteogenic differentiation [127] through the stiffness-induced expression of osteoblast markers, such as RUNX2, a helix-loop-helix nuclear factor that initiates the osteogenic differentiation of MSCs [128]. In addition, ALP is also highly excreted during osteogenic differentiation [126], and OCN is highly expressed during the late osteogenesis stage [91]. In mature osteoblast, cells also deposit calcium phosphate into the ECM [91]. The response of MSCs to ECM stiffness depends on integrins, the cytoskeleton, and cross-talk among various signal transduction pathways. Integrin binding and cytoskeletal organization in MSCs can vary depending on the stiffness of the ECM. On stiff ECM, cells transmit mechanical stimuli through the axis of α2 integrin-ROCK-FAK-ERK1/2, which increases RUNX2 activity, resulting in the osteoblast differentiation of MSCs [129]. In summary, hADSCs that were cultured on the stiffer PEEU70 scaffold demonstrated a preference for osteogenesis compared to cells grown on the softer PEEU fiber meshes (PEEU40, PEEU50, or PEEU60).

Chapter 5

Conclusions and Outlook

5.1 Conclusions

Biomaterials are substances that are designed to engage with biological systems in a medical setting [41]. Biomaterials might derive from nature or be manufactured in the laboratory and can be utilized in a wide range of medical applications to support, enhance, or replace damaged tissue or to restore biological functions. Currently, biomaterials are primarily used in the form of sutures, scaffolds for medical devices, tissue regeneration, and controlled drug delivery systems [42-45]. To fulfil these applications, biomaterials must feature specific characteristics, including (1) non-toxicity, (2) an appropriate biodegradation rate, (3) suitable mechanical properties [47], (4) the ability to be modified to meet the requirement of the required task, (5) and good biocompatibility [46].

Previously, the multiblock copolymer PDC was synthesized at our institute through the combination of PPDO segments and PCL segments using HDI as a linker. In the final polymer, PDC was obtained with a number-average molecular weight of 75 kg·mol^{-1}. PDC has low glass transition temperatures, which aid in the formation of elastic materials at body temperatures. PDC is a viscoelastic and flexible polymer and represents a promising candidate for implantation applications. PDC films presented low Young's modulus (20 ± 1 MPa) values and high elongation at break values ($\varepsilon_b = 420 \pm 30\%$) [70]. The characterized PDC film was found to be a hydrophilic material with a water contact angle of $63 \pm 4°$ [70]. *In vitro*, PDC was found to have EC-selective adhesion properties, simultaneously suppressing the attachment of smooth muscle cells [70]. Together, these findings indicated that PDC might serve as a good candidate for use in implantation designed to restore blood vessels [71]. PDC films might possess angiogenic potential *in vivo*, and has been shown to promote the formation of blood vessels in a rat neck and the chorioallantoic membrane of a chicken egg [74, 75]. In summary, hydrophilicity, low thrombogenicity [76], the selective enhancement of EC adhesion [70, 71], and pro-angiogenic properties [74, 75] combined to indicate that PDC may represent a desirable candidate for blood-interacting uses, such as vascular grafts or EC-selective' stents.

In this thesis, PEEU, composed of PPDO and PCL segments using LDI as a linker, was synthesized. Compared with the HDI linker used in PDC, LDI has improved biocompatibility, and LDI-based polymers possess reduced cytotoxicity and better hemocompatibility than HDI-based polymers [94]. The presence of additional hydrogen bonding groups on the ethyl ester side group of LDI may improve the hydrophilicity of LDI-based polymers compared with HDI-based polymers [95].

The degradability, the thermal features, and stiffness of PDC can be adjusted by varying the PPDO proportion, and lowering the PPDO wt.% lowered the *E*-modulus and increased the elongation at break. In this thesis, four types of PEEU were synthesized using various PPDO weight ratios, ranging between 40 wt.%. and 70 wt.%.

The biomimetic properties of 3D scaffolds are better than those of 2D substrates because cells are exposed to 3D microenvironments *in vivo*. Moreover, 3D scaffolds, by mimicking the *in vivo* environment, can possess desirable mechanical properties, high porosity and interconnectivity, which can be used to incorporate cells and implant them into the human body to enhance new tissue formation with limited inflammatory reactions [96]. In addition, fibrous PDC scaffolds were shown to behave similar to a textile, adapting to the curvature of tissue found at the implantation site better than rigid films. Furthermore, HUVECs cultured on micron-scale fibers (2 µm) showed higher adhesion and improved proliferation and viability properties compared with HUVECs cultured on submicron-scale fibers (0.5 µm). Therefore, micron-scale PDC fibers are considered to be a more promising candidate material for blood-contacting biomaterial applications compared with submicron-scale fibers [107]. For this reason, PEEU scaffolds with micron-sized single fibers (1.4 – 1.7 µm) were fabricated using electrospinning method.

During this study, PEEU scaffolds containing micron-scale fibers (approximately 1.5 µm) and similar porosity characteristics (60%) were prepared. The thermal properties of these PEEU polymers scaffolds were examined in a previously reported work [107]. The PEEU scaffolds exhibited a low glass transition temperature and two melting transition temperatures, at 41°C and 92°C, which were similar to those reported for PDC [73]. The glass transition temperatures were below body temperature, indicating that PEEU scaffolds are soft and elastic materials, that may be promising candidates for body implantation applications. The stiffness of PEEU scaffolds could be increased by increasing the proportions of PPDO segments, and a significant

difference in the stiffness was identified between PEEU70 and PEEU40. Difference in the *E*-modulus of PEEU scaffolds might influence cell behaviors.

In Section 4.2, the potential use of these fiber mesh scaffolds for angiogenesis applications was determined by evaluating the adhesion, migration, growth, and angiogenesis potential of ECs. The results of this study supported the theory that ECs are sensitive to the elasticity of materials. HUVECs responded differently to fiber meshes made from PEEU materials with varying stiffness. The cells cultured on PEEU70 fiber mesh scaffolds presented elongated morphologies, promoted cell proliferation and enhanced migratory capabilities, and promoted angiogenesis abilities. The fiber meshes derived using PEEU70 may serve as a promising candidate for blood vessel regeneration. In addition, this study was able to provide meaningful insights into the design and constructing of function-oriented biomimetic fiber meshes designed to promote vascular regeneration and repair in the future.

In Section 4.3, the effects of stiffness of different PEEU fiber meshes on the osteogenesis differentiation potential of hADSCs were explored by measuring the protein expression levels of osteogenic differentiation markers. The results demonstrated that cells cultured on the stiffer fiber meshes (e.g. PEEU70) showed elongated cell shapes and the higher nuclear aspect ratios compared with cells cultured on softer fiber meshes (e.g. PEEU40). The increased stiffness of the PEEU fiber mesh significantly promoted the osteogenic differentiation of hADSCs. The results from this study provided insights into the production of function-oriented biomimetic fiber meshes designed to promoted bone regeneration.

In summary, this study compared four types of PEEU scaffolds with different E-modulus. PEEU scaffolds generation was optimized to produce similar micron-scale fiber diameters and high porosity characteristics. The PEEU scaffolds showed high elongation potential and were soft and elastic when used at human body temperature. PEEU70 scaffolds containing desirable stiffness could be used to promote the angiogenic potential of ECs and could be used as biomimetic fibrous implants to improve vascular regeneration in the human body. These results provided understandings into the production of function-oriented fiber meshes designed to enhance bone regeneration.

5.2 Outlook

5.2.1 Degradation behavior of PEEU electrospun scaffolds

The degradability of a polymer is essential for use in biomaterial-based regenerative therapies, such as the repair or replacement of articular cartilage defects [72]. The degradability of PDC could be adjusted by altering the PPDO composition. PDC was found to experience a linear mass loss in both hydrolytic and enzymatic degradation process, and the degradability could be modulated by changing the weight ratio between PPDO and PCL in the polymer and by adjusting the surface to volume ratio [72, 73]. The reported methods used during these PDC degradation experiments could be performed using our present 3D PEEU scaffolds in future experiments.

5.2.2 Effects of the fiber orientation of PEEU fiber meshes on endothelial cell behaviors

The alignment of mesh fibers has been shown to increase HUVEC proliferation rate while reduces cell viability of HUVEC and SMC [107]. Compared with randomly oriented fibers, aligned PDC fibers scaffolds were shown to promote angiogenesis, resulting in the formation of new vessels 28 day after implantation, suggesting that the parallel arrangement fibers may be a method for the development of biomaterial candidates for use in regenerative applications [130]. In summary, aligned fibers might be used as desirable structural signals to influence the formation and orientation of newly formed blood vessels.

In future experiments, the use of aligned PEEU fiber scaffolds warrants exploration in comparison with randomly oriented fibers scaffolds to achieve an in-depth understanding of how highly aligned microenvironment architectures might impact HUVEC angiogenesis.

5.2.3 Evaluation of the effects of PEEU scaffolds on the angiogenic potential *in vivo*

In Section 4.2, an *in vitro* evaluation of the angiogenic potential of PEEU scaffolds was performed. The results implied that the PEEU70 fiber meshes possessed a greater proangiogenic potential than the other tested substrates. Compared with *in vitro* systems, the *in vivo* microenvironment is dynamic, and some tissues, such as articular cartilage, exist in

low-oxygen environments. Future studies should evaluate the angiogenesis potential of PEEU fiber scaffolds *in vivo*.

5.2.4 PEEU scaffolds for stem cell osteogenic differentiation

In Section 4.3, we demonstrated that hADSCs cultured on stiffer PEEU electrospun scaffolds preferentially underwent osteogenic differentiation. These results suggest that the PEEU70 scaffold successfully enhanced hADSCs osteogenic differentiation and implied the potential use of PEEU70 in applications intended to incorporate hADSCs for the therapy of bone defects. However, the lack of a vascular supply could result in decreased cell viability and implant failure [131]. Hence, approaches that could be used to vascularize the scaffold must be explored during future investigations, such as the co-culture of ECs and osteoblasts in the optimized biomaterial scaffolds [132].

Chapter 6

Experimental section

6.1   Materials

PEEU multiblock copolymers, composed of PPDO diols and PCL diols [22]. PEEU(x) is a copolymerization of x wt.% PPDO and (100-x) wt.% PCL segments. The composition of PEEU was varied, and the weight ratio of the PPDO segments ranged between 40 wt.% and 70 wt.%, resulting in the synthesis of four types of PEEU co-polymers materials, referred to as PEEU40, PEEU50, PEEU60, and PEEU70. The multiblock polymers were provided by Dr. Karl Kratz, Dr. Michael Zierke, and Monique Hannemann from our institute.

6.2   Preparation of polymer scaffolds using the electrospinning method

The electrospinning of the fiber meshes work was performed by Wingtai Tung at HZG institute. The fiber meshes derived from different PEEU materials were prepared using the electrospinning method. PEEU materials were first dissolved in hexafluoroisopropanol solvent, according to the concentration shown in Table 1. The resulting polymer solution was used to fill a syringe and was filtered through a 1 µm pore membrane before undergoing electrospinning. The electrospinning process was carried out inside a custom-made chamber with controlled humidity, which was maintained at 20% for the electrospinning of PEEU fibers. The PEEU solution was electrospun at a flow rate of 2.12 ml/h and a tip- to- collector distance of 25 cm. The collector was a revolving drum wrapped with polypropylene film. To obtain a steady Taylor cone, the applied voltage for electrospinning was varied throughout the operation, as shown in Table 6-1. The entire duration of PEEU fiber mesh preparation using the electrospinning method was approximately 4 h.

Table 6-1 Electrospinning conditions used to generate PEEU materials

	Concentration (wt%)	Flow rate (mL/h)	TCD (cm)	Voltage (kV)	Drum rotation (rpm)	Duration (h)
PEEU40	11	2.121	25	16~18	10	4
PEEU50	11	2.121	25	20~21	10	4
PEEU60	11	2.121	25	20~21	10	4
PEEU70	11	2.121	25	14~15	10	4

Abbreviations: TCD, tip to collector distance.

6.3   Sterilization of scaffolds

Before performing the other experiments, the obtained fiber meshes generated from PEEU materials were sterilized by ethylene oxide method with 10 vol.% ethylene oxide, at 54 °C, 65% relative humidity, 1.7 bar pressure, 3 hours of gas exposure time, and 21 hours of aeration. The sterilization was performed by Mario Rettschlag at HZG institute.

6.4   Characterizations

6.4.1 SEM imaging and analysis

The surface morphologies of the PEEU fiber mesh were examined using a SEM (Phenom G2 pro, L.O.T.–Oriel, Darmstadt, Germany). First, the PEEU fiber meshes were placed in a vacuum oven overnight and coated with 5 nm gold in sputter coater (Polaron SC7640) and then were observed at room temperature. The obtained SEM images for the four different samples were examined using Image J software version 1.44 (National Institutes of Health) [23]. 100 individual fibers from each sample were measured to determine the average diameter and diameter variation. [24].

6.4.2 Thermal characterization of PEEU fiber meshes by DSC

DSC experiments were carried out with a Netzsch DSC 204 (NETZSCH-Geratebau GmbH,

Selb/Bavaria, Germany) to characterize the thermal properties of the PEEU fiber mesh scaffolds. 5 mg was weighed for each sample and sealed into an aluminum pan. The experiment was carried on under nitrogen-atomosphere with a constant heating and cooling rate of 10 ℃·min^{-1}. The first heating, cooling, and second heating curves, temperature were range from room temperature to 150 ℃, 150 ℃ to -100 ℃, and -100 ℃ to 150 ℃ respectively. The samples were first heated up to 150 ℃ and hold for 10 min to erase the heat history, and then cooled to -100 ℃ with another 10 min holding stage, followed by reheating to 150 ℃ again. An empty aluminum pan was employed as a reference.

The melting and glass transition temperature were determined by the second heating curve and cooling curve, respectively.

6.4.3 Mechanical properties analysis

A tensile testing method was used to characterize the mechanical characteristics of the fiber mesh made from PEEU components. The tensile test was carried out inside a temperature chamber of tensile test apparatus (Zwick GmbH, Ulm, Germany) at 37 °C under dry conditions. The fiber meshes (n = 5, mean ± SD) were punched into 1 cm × 4 cm strips. Samples were clamped and equilibration at 37 °C in the temperature chamber before the experiment.

6.5   PEEU fiber mesh pre-treatment before cell culture

For cell culture experiments, PEEU fiber mesh scaffolds were first punched into round shaped samples with a diameter of 12 mm using a Biopsy Punch (Thermo Fisher Scientific, Waltham, USA) and Sterilization bags were used to pack the items, which were then sterilized. using ethylene oxide method as described in section 6.3.

The PEEU fiber meshes were placed into the wells of 24-well plate (shown in Figure 3-1) and were washed 3 times using PBS before cell culture.

6.6   HUVEC characterization

The morphology of HUVECs (Lonza, Walkersville, MD, USA) was viewed and captured using AxioVision rel. 4.8 software (Carl Zeiss, Jena, Germany). A flow cytometer (MACSQuant®, Miltenyi Biotec, Bergisch Gladbach, Germany) was used to assess cell phenotypes. HUVECs were fixed for 15 minutes at room temperature in 4 (w/v) % paraformaldehyde (PFA), then permeabilized for 10 minutes with 0.2 vol. % Triton X-100 buffer (Sigma), and incubated with rabbit anti-human vWF antibody (DakoCytomation, Denmark), followed by staining with a panel of FITC- or PE-conjugated anti-human CD31 (Miltenyi). The corresponding fluorochrome-conjugated isotype antibody was used as the negative control. FlowJo software was used to process the data. (Tree Star Inc., Ashland OR, USA).

6.7   Cultivation of HUVECs

HUVECs (Lonza, Walkersville, MD, USA) were grown in an EC growth medium (EGM^{TM}, Lonza, Walkersville, MD, USA) at 37 °C in a humidified environment containing 5 vol.% CO_2 in a cell culture incubator. Every other day, the medium was replaced, and non-adherent cells were eliminated. HUVECs were subcultured into fresh flasks after they had attained approximately 90% confluence in the culture flasks, using 0.25 vol.% trypsin–EDTA solution.

6.8   Cell seeding

The HUVECs were seeded at a selected density in 1 mL media onto electrospun fiber meshes previously placed in 24-well culture plates. The cells were allowed to attach to the fiber meshes overnight, and then the media was replaced with 1 ml of new culture media. The cells were incubated at 37 °C with 5 vol.% CO_2 in a humidified environment.

6.9   Immunostaining assay

After a selected culture time, HUVECs were examined by immunofluorescence to determine the presence of cell markers. The cells were first fixed for 20 min at room temperature with 4 vol.% paraformaldehyde (Sigma–Aldrich, St. Louis, USA) and then permeabilized for 15 min

with 0.2 vol.% Triton X-100 (Sigma–Aldrich, St. Louis, MO, USA). After washing with PBS, They were stained for 30 min at room temperature with ActinRed™ 555 (Life Technologies, Darmstadt, Germany) to identify the cytoskeleton and Hoechst 33342 (NucBlue® Live Reagent, Life Technologies, Darmstadt, Germany) to identify the nucleus. The cells were washed three times with $1\times$ PBS, each time for 10 min. After that, the samples were then mounted and examined using a confocal laser scanning microscope (LSM 780, Carl Zeiss, Jena, Germany).

6.10 HUVEC morphology assessment method

HUVECs were seeded at a density of 5.0×10^4 per 1 cm^2 onto the various electrospun PEEU fiber meshes to analyze cell shape. After 3 days of culture, The cells were fixed for immunofluorescence staining. Image J was used to examine the cell aspect ratios (National Institutes of Health, USA).

6.11 HUVEC proliferation method

The Cell Counting Kit-8 test was used to count the number of HUVECs cultivated on fiber meshes made from PEEU materials (CCK-8; Dojindo Laboratories, Kumamoto, Japan). HUVECs were seeded onto the PEEU fiber meshes at a density of 1×10^5 cells per fiber mesh scaffold. At selected time points after cell seeding (1, 3, 6, and 9 days post-seeding), the culture media were replaced with culture media containing 10 vol.% CCK-8 solution, and the samples were incubated for 2 h at 37 °C. Then, the absorbance at 450 nm was measured using a microplate reader (Biotek, Winooski, VT, USA), and cell numbers were calculated using a standard curve.

6.12 HUVEC migration method

To analyze the migration of HUVECs, 1×10^4 live cells were first seeded onto the various fiber meshes generated using PEEU materials. After 7 days of culture, the cells were collected with 0.25 vol.% trypsin and EDTA solutions, and reseeded into the wells of a 24-well tissue culture plate at a concentration of 2.0×10^4 per milliliter of growth media. The nuclei of the cells were

then dyed in cell growth media with Hoechst 33342 nuclear dye (NucBlue[TM] Live ReadyProbes[TM] Reagent, Thermofisher scientific, Eugene, OR USA) to image cells for tracking analysis. The medium was replaced, and cell migration was monitored by a time lapse microscopy, a IX81 motorized inverted optical microscopy (Olympus Co., Hamburg, Germany) with a enclosure incubator suitable for a 24-well plate to maintain cell growth at 37 °C in a humidified environment containing 5 vol.% CO_2. For more than 15 hours, Cell movement was monitored. Image J program (National institutes of health, United states of America) was used to assess the migratory paths and velocities, together with the 'chemotaxis and migration tool' and 'manual tracking' software plugins (ibidi GmbH, Martinsried, Germany).

6.13 Tube formation assay for HUVECs

The cells used to perform the tube formation assay were collected from cultures grown onto all the various PEEU fiber meshes for a week. The wells of a 24 wells cell culture plate were initially treated with the Geltrex Matrix reagent (Life Technologies, Darmstadt, Germany), as recommended by the manufacturer, 200 µL Geltrex Matrix reagent was used for each well to measure the tube development of HUVECs. The Geltrex Matrix pre-treated wells were then seeded with 7×10^4 HUVECs. For each well, medium was added to each well to bring the total volume to 500 µL. The generated closed tubes and total tubes length were recorded using AxioVision rel. 4.8 software (Carl Zeiss, Jena, Germany) after 18 hours of incubation. The number of established enclosed tubes was observed, and the length of the total tubes was calculated by Image J software (National institutes of Health, USA) coupled with the software plugin 'Angiogenesis Analyzer' in each well after pictures were obtained in randomly selected observation areas.

6.14 Human adipose-derived stem cells (hADSCs) isolation and culture

Human adipose tissue was acquired from a female donor who underwent abdominal liposuction surgery and was obtained with the consent of the donor for use in research (No.: EA2/127/07; Ethics Committee of the Charité Universitätsmedizin, Berlin, permission dated 17th.Oct.2008).

The isolation and culture of hADSCs from human adipose tissues was carried out as mentioned earlier [133].

The hADSCs were expanded at 37 °C in hADSC culture medium (ADSC^{TM} growth medium, Lonza, Walkersville, MD, USA) in a humidified environment incubator with 5 vol.% CO_2. Following incubation, the media was changed every two days until the cells achieved approximately 90% confluence. The cells were then digested with 0.25 vol.% trypsin–EDTA solution, separated at 300 ×g for 5 minutes, re-suspended in culture media, and seeded in new flasks.

6.15 Assay of cell viability

And in accordance with the manufacturer's instructions, a LIVE/DEAD® Viability and Cytotoxicity Kit for mammalian cells (Invitrogen, Carlsbad, CA, USA) was used to measure cell viability. cells were planted onto the PEEU fiber mesh scaffolds (2×10^5 cells per scaffold). Cell viability was evaluated 7 days after culture by exposing cells to a LIVE and DEAD reagent (4 mM Calcein AM-green; live cells and 2 mM Ethidium homodimer-1-red; dead cells) for 30 minutes at room temperature. After that, the cells were examined using a laser scanning microscopy (Carl Zeiss, Oberkochen, Germany).

6.16 Morphology of hADSCs and their nuclei

hADSCs were planted onto PEEU fiber meshes at a density of 5.0×10^4 per square centimeter and fixed with 4 (w/v) % paraformaldehyde after three days culture to evaluate cell and nuclear morphology following culture on the fiber meshes surface. Image J (National Institutes of Health, USA) software was used to assess the cell and nuclear morphology after they were cultivated on the scaffold material surface. Area and circumference measurements were obtained by manually tracing cell boundaries using NIH ImageJ software.

6.17 Differentiation assay

For the differentiation study, $1 \times 10^5 / cm^2$ hADSCs were seeded onto the PEEU fiber meshes. The scaffolds were shifted to a new well of a 24-well plate after three days of culture,. Then,

the cells were incubated in a 1:1 (v/v) ratio of osteogenic (StemPro Osteogenesis differentiation kit) and adipogenic (StemPro Adipogenesis differentiation kit) induction media. Every three days, the induction media were replaced. The cells were grown in the mixed induction media for three weeks to evaluate the hADSC osteogenic differentiation. The samples were then fixed for 15 minutes at room temperature with 4 (w/v) % paraformaldehyde, permeabilized for 10 minutes with 0.2 vol. % Triton X-100 solution, and stained. Area and circumference measurements were obtained by manually tracing cell boundaries using NIH ImageJ software.

6.18 Alkaline phosphatase assay

For three weeks, hADSCs on all various PEEU fiber meshes were grown in the mixed competitive differentiation media. The cells were lysed and the supernatant was collected for use in an alkaline phosphatase test kit (Abcam, Berlin, Germany), which employs p-nitrophenyl phosphate (pNPP) as a phosphatase substrate. 30 µL of the cell lysate was added in a 96-wells plate. Upon addition of 50 µL assay buffer and 50 µL pNPP, plates were protected from direct light and incubated at ambient temperature for 1 h. Finally, 20 µL Stop Solution (3N NaOH) were added to stop the reaction. Tecan Infinite® 200 PRO microplate reader (Tecan Deutschland GmbH, Germany) measured the plate at 405 nm. The total protein quantity was used to normalize the data.

6.19 Osteocalcin expression assay

The osteogenesis of hADSCs on all various PEEU fiber meshes was also investigated utilizing an enzyme-linked immunosorbent test (ELISA) to measure osteocalcin (OCN) expression. The hADSCs were grown for three weeks in the mixed competitive differentiation media for three weeks before being lysed with a RIPA lysis and extraction solution (Thermo Fisher Scientific, Massachusetts, USA) including a cocktail of 1× halt protease and phosphatase inhibitors cocktail (Thermo Fisher Scientific, Massachusetts, USA). The protein in the supernatant was collected and quantified with a BCA protein assay kit (Thermo Fisher Scientific, Bonn, Germany) after the lysate was centrifuged at 15000 ×g for 15 minutes. The human osteocalcin ELISA kit (Invitrogen, California, USA) was used to quantify the osteocalcin in the supernatant, which was standardized by the quantify of total protein determined using a BCA protein assay

6.20 Mineralization assay

Osteogenesis could also be determined by staining with the OsteoImage™ Mineralization Assay kit (Lonza, Walkersville, MD, USA), which can be carried out to visually detect and quantitate in vitro mineralization by osteogenic stem cells. The hADSCs on the PEEU fiber meshes were grown in the mixed competitive differentiation medium for three weeks and then were fixed with 4% (w/v) paraformaldehyde (Thermo Fisher Scientific, Waltham, USA) for 20 minutes. Samples were stained with OsteoImage™ Staining Reagent (Lonza, Walkersville, MD, USA) in the dark at room temperature for 30 minutes and Hoechst 33342(Life Technologies, Darmstadt, Germany) was used to stan the cell nucleus of each well. The stained samples were scanned using a confocal laser scanning microscopy (LSM 780, Carl Zeiss, Jena, Germany) after being rinsed three times with 1× PBS and then. Image J software (National Institutes of Health, USA) was used to do a quantitative measurement of the fluorescence intensity of the stained hydroxyapatite. The fluorescence intensity was normalized by the cell number.

6.21 RUNX2 immunostaining

hADSCs on fiber mesh scaffolds were cultured for the designated number of days, then fixed for 15 minutes with 4 (w/v) % paraformaldehyde (Sigma), permeabilized for 10 minutes with 0.25 (v/v) % Triton X-100 (Sigma), and blocked for 1 hour at room temperature with 5 (w/v) % BSA (Invitrogen) in 1× PBS. Primary antibodies RUNX2 (mouse monoclonal, Abcam, Berlin, Germany) were incubated for 4 hours at room temperature before being washed three times with 1 × PBS for 10 minutes each time. Then, at room temperature, a secondary antibody (Thermo Fisher Scientific, Schwerte, Germany) was added and incubated for 1 hour. Hoechst 33342 (Life Technologies, Darmstadt, Germany) was used to stain the nuclei for 20-30 minutes at room temperature. A laser scanning confocal microscopy (LSM710, Carl Zeiss, Germany) was used to examine the fluorescence images. RUNX2 nuclear localization was analyzed by comparing fluorescence intensity in the nucleus and cytoplasm of each cell using ImageJ (National Institutes of Health). Cells with nuclear/cytoplasm fluorescence ratio > 1.5 were defined as RUNX2 active cells.

6.22 Statistical analysis and error consideration

A two-tailed independent-samples t-test was used to compare the two groups statistically. One-way analysis of variance (ANOYA) was used to assess differences among three or more independent groups, followed by Tukey's multiple comparisons test. GraphPad Prism software (Version 7.04, GraphPad Software, Inc., San Diego, CA, USA) was used to conduct the statistical analysis. Statistical significance was defined as a $p < 0.05$ level of significance. The number of repetitions for each experiment is reflected in the figure legends for each test. Data are showed as the mean and standard deviation. The error related to methods was estimated as: $\pm 0.5 \,^{\circ}\text{C}$ for temperature controller for DSC.

References

1. Frantz, C., K.M. Stewart, and V.M. Weaver, *The extracellular matrix at a glance.* Journal of cell science, 2010. **123**(Pt 24): p. 4195-4200.

2. Lane, S.W., D.A. Williams, and F.M. Watt, *Modulating the stem cell niche for tissue regeneration.* Nat Biotechnol, 2014. **32**(8): p. 795-803.

3. Murphy, W.L., T.C. McDevitt, and A.J. Engler, *Materials as stem cell regulators.* Nat Mater, 2014. **13**(6): p. 547-57.

4. Crowder, S.W., et al., *Material Cues as Potent Regulators of Epigenetics and Stem Cell Function.* Cell Stem Cell, 2016. **18**(1): p. 39-52.

5. Frantz, C., K.M. Stewart, and V.M. Weaver, *The extracellular matrix at a glance.* J Cell Sci, 2010. **123**(Pt 24): p. 4195-200.

6. Bonnans, C., J. Chou, and Z. Werb, *Remodelling the extracellular matrix in development and disease.* Nat Rev Mol Cell Biol, 2014. **15**(12): p. 786-801.

7. Schedin, P. and P.J. Keely, *Mammary gland ECM remodeling, stiffness, and mechanosignaling in normal development and tumor progression.* Cold Spring Harb Perspect Biol, 2011. **3**(1): p. a003228.

8. Lu, P., et al., *Extracellular matrix degradation and remodeling in development and disease.* Cold Spring Harb Perspect Biol, 2011. **3**(12).

9. Yeh, Y.T., et al., *Matrix stiffness regulates endothelial cell proliferation through septin 9.* PLoS One, 2012. **7**(10): p. e46889.

10. Ataollahi, F., et al., *Endothelial cell responses in terms of adhesion, proliferation, and morphology to stiffness of polydimethylsiloxane elastomer substrates.* J Biomed Mater Res A, 2015. **103**(7): p. 2203-13.

11. Iskratsch, T., H. Wolfenson, and M.P. Sheetz, *Appreciating force and shape — the rise of mechanotransduction in cell biology.* Nature Reviews Molecular Cell Biology, 2014. **15**(12): p. 825-833.

12. Broders-Bondon, F., et al., *Mechanotransduction in tumor progression: The dark side of the force.* Journal of Cell Biology, 2018. **217**(5): p. 1571-1587.

13. Alonso, J.L. and W.H. Goldmann, *Cellular mechanotransduction.* AIMS Biophysics, 2016. **3**(1): p. 50-62.

14. Martinac, B., *The ion channels to cytoskeleton connection as potential mechanism of mechanosensitivity.* Biochimica et Biophysica Acta (BBA) - Biomembranes, 2014. **1838**(2): p. 682-691.

15. Nicolas, J., et al., *3D Extracellular Matrix Mimics: Fundamental Concepts and Role of Materials Chemistry to Influence Stem Cell Fate.* Biomacromolecules, 2020. **21**(6): p. 1968-1994.

16. Marsico, G., et al., *Glycosylation and Integrin Regulation in Cancer.* Trends in Cancer, 2018. **4**(8): p. 537-552.

17. Lee, J., et al., *Geometric guidance of integrin mediated traction stress during stem cell differentiation.* Biomaterials, 2015. **69**: p. 174-183.

18. Tsimbouri, P.M., et al., *A genomics approach in determining nanotopographical effects on MSC phenotype.* Biomaterials, 2013. **34**(9): p. 2177-2184.

19. and, K.B. and M. Chrzanowska-Wodnicka, *FOCAL ADHESIONS, CONTRACTILITY, AND SIGNALING.* Annual Review of Cell and Developmental Biology, 1996. **12**(1): p. 463-519.

20. Dahl, K.N., A.J.S. Ribeiro, and J. Lammerding, *Nuclear shape, mechanics, and mechanotransduction.* Circulation research, 2008. **102**(11): p. 1307-1318.

21. Chancellor, T.J., et al., *Actomyosin tension exerted on the nucleus through nesprin-1 connections influences endothelial cell adhesion, migration, and cyclic strain-induced reorientation.* Biophys J, 2010. **99**(1): p. 115-23.

22. Lombardi, M.L., et al., *The interaction between nesprins and sun proteins at the nuclear envelope is critical for force transmission between the nucleus and cytoskeleton.* J Biol Chem, 2011. **286**(30): p. 26743-53.

23. Maniotis, A.J., C.S. Chen, and D.E. Ingber, *Demonstration of mechanical connections between integrins, cytoskeletal filaments, and nucleoplasm that stabilize nuclear structure.* Proc Natl Acad Sci U S A, 1997. **94**(3): p. 849-54.

24. Lovett, D.B., et al., *Modulation of Nuclear Shape by Substrate Rigidity.* Cellular and molecular bioengineering, 2013. **6**(2): p. 230-238.

25. McNamara, L.E., et al., *Nanotopographical control of stem cell differentiation.* J Tissue Eng, 2010. **2010**: p. 120623.

26. Guilak, F., et al., *Control of stem cell fate by physical interactions with the extracellular matrix.* Cell Stem Cell, 2009. **5**(1): p. 17-26.

27. Yim, E.K., et al., *Nanotopography-induced changes in focal adhesions, cytoskeletal organization, and mechanical properties of human mesenchymal stem cells.* Biomaterials, 2010. **31**(6): p. 1299-306.

28. Yim, E.K., S.W. Pang, and K.W. Leong, *Synthetic nanostructures inducing differentiation of human mesenchymal stem cells into neuronal lineage.* Exp Cell Res, 2007. **313**(9): p. 1820-9.

29. Dalby, M.J., et al., *The control of human mesenchymal cell differentiation using nanoscale symmetry and disorder.* Nature Materials, 2007. **6**(12): p. 997-1003.

30. McMurray, R.J., et al., *Nanoscale surfaces for the long-term maintenance of mesenchymal stem cell phenotype and multipotency.* Nature Materials, 2011. **10**(8): p. 637-644.

31. Tsimbouri, P.M., et al., *Using Nanotopography and Metabolomics to Identify Biochemical Effectors of Multipotency.* ACS Nano, 2012. **6**(11): p. 10239-10249.

32. Takahashi, T., et al., *Three-Dimensional Microenvironments Retain Chondrocyte Phenotypes During Proliferation Culture.* Tissue Engineering, 2007. **13**(7): p. 1583-1592.

33. McBeath, R., et al., *Cell Shape, Cytoskeletal Tension, and RhoA Regulate Stem Cell Lineage Commitment.* Developmental Cell, 2004. **6**(4): p. 483-495.

34. Le Beyec, J., et al., *Cell shape regulates global histone acetylation in human mammary epithelial cells.* Experimental Cell Research, 2007. **313**(14): p. 3066-3075.

35. Chowdhury, F., et al., *Material properties of the cell dictate stress-induced spreading and differentiation in embryonic stem cells.* Nat Mater, 2010. **9**(1): p. 82-8.

36. Park, J.S., et al., *The effect of matrix stiffness on the differentiation of mesenchymal stem cells in response to TGF-beta.* Biomaterials, 2011. **32**(16): p. 3921-30.

37. Engler, A.J., et al., *Matrix elasticity directs stem cell lineage specification.* Cell, 2006. **126**(4): p. 677-89.

38. Discher, D.E., P. Janmey, and Y.L. Wang, *Tissue cells feel and respond to the stiffness of their substrate.* Science, 2005. **310**(5751): p. 1139-43.

39. Kim, S.N., et al., *ECM stiffness regulates glial migration in Drosophila and mammalian glioma models.* Development, 2014. **141**(16): p. 3233.

40. Swift, J., et al., *Nuclear Lamin-A Scales with Tissue Stiffness and Enhances Matrix-Directed Differentiation.* Science, 2013. **341**(6149): p. 1240104.

41. Williams, D.F., *On the nature of biomaterials.* Biomaterials, 2009. **30**(30): p. 5897-5909.

42. Fenton, O.S., et al., *Advances in Biomaterials for Drug Delivery.* Adv Mater, 2018: p. e1705328.

43. Kohane, D.S. and R. Langer, *Polymeric Biomaterials in Tissue Engineering.* Pediatric Research, 2008. **63**(5): p. 487-491.

44. Zagho, M.M., E.A. Hussein, and A.A. Elzatahry, *Recent Overviews in Functional Polymer Composites for Biomedical Applications.* Polymers, 2018. **10**(7): p. 739.

45. Qasim, S.B., et al., *Electrospinning of Chitosan-Based Solutions for Tissue Engineering and Regenerative Medicine.* Int J Mol Sci, 2018. **19**(2).

46. Lendlein, A. and A. Sisson, *Handbook of biodegradable polymers: isolation, synthesis, characterization and applications*. 2011: John Wiley & Sons. p. 1-21.

47. Liu, H., et al., *Recent studies on electrospinning preparation of patterned, core–shell, and aligned scaffolds.* Journal of Applied Polymer Science, 2018. **135**(31): p. 46570.

48. Vert, M., *Degradable and bioresorbable polymers in surgery and in pharmacology: beliefs and facts.* Journal of Materials Science: Materials in Medicine, 2009. **20**(2): p. 437-446.

49. Pant, B., M. Park, and S.J. Park, *Drug Delivery Applications of Core-Sheath Nanofibers Prepared by Coaxial Electrospinning: A Review.* Pharmaceutics, 2019. **11**(7).

50. Thakkar, S. and M. Misra, *Electrospun polymeric nanofibers: New horizons in drug delivery.* Eur J Pharm Sci, 2017. **107**: p. 148-167.

51. Wang, X., et al., *Electro-spinning/netting: A strategy for the fabrication of three-dimensional polymer nano-fiber/nets.* Progress in Materials Science, 2013. **58**(8): p. 1173-1243.

52. Haider, A., S. Haider, and I.-K. Kang, *A comprehensive review summarizing the effect of electrospinning parameters and potential applications of nanofibers in biomedical and biotechnology.* Arabian Journal of Chemistry, 2018. **11**(8): p. 1165-1188.

53. Shahriar, S.M.S., et al., *Electrospinning Nanofibers for Therapeutics Delivery.* Nanomaterials (Basel), 2019. **9**(4).

54. Ramakrishna, S., et al., *Electrospun nanofibers: solving global issues.* Materials Today, 2006. **9**(3): p. 40-50.

55. Deitzel, J.M., et al., *Controlled deposition of electrospun poly(ethylene oxide) fibers.* Polymer, 2001. **42**(19): p. 8163-8170.

56.   Mochane, M.J., et al., *Morphology and Properties of Electrospun PCL and Its Composites for Medical Applications: A Mini Review.* Applied Sciences, 2019. **9**(11): p. 2205.

57.   Cipitria, A., et al., *Design, fabrication and characterization of PCL electrospun scaffolds—a review.* Journal of Materials Chemistry, 2011. **21**(26): p. 9419-9453.

58.   Bhattarai, S.R., et al., *Novel biodegradable electrospun membrane: scaffold for tissue engineering.* Biomaterials, 2004. **25**(13): p. 2595-602.

59.   Yoshimoto, H., et al., *A biodegradable nanofiber scaffold by electrospinning and its potential for bone tissue engineering.* Biomaterials, 2003. **24**(12): p. 2077-82.

60.   Shin, M., H. Yoshimoto, and J.P. Vacanti, *In vivo bone tissue engineering using mesenchymal stem cells on a novel electrospun nanofibrous scaffold.* Tissue Eng, 2004. **10**(1-2): p. 33-41.

61.   Tuzlakoglu, K., et al., *Nano- and micro-fiber combined scaffolds: a new architecture for bone tissue engineering.* J Mater Sci Mater Med, 2005. **16**(12): p. 1099-104.

62.   Li, W.J., et al., *Fabrication and characterization of six electrospun poly(alpha-hydroxy ester)-based fibrous scaffolds for tissue engineering applications.* Acta Biomater, 2006. **2**(4): p. 377-85.

63.   Yao, Q., et al., *Three dimensional electrospun PCL/PLA blend nanofibrous scaffolds with significantly improved stem cells osteogenic differentiation and cranial bone formation.* Biomaterials, 2017. **115**: p. 115-127.

64.   Xu, C.Y., et al., *Aligned biodegradable nanofibrous structure: a potential scaffold for blood vessel engineering.* Biomaterials, 2004. **25**(5): p. 877-86.

65.   Mo, X.M., et al., *Electrospun P(LLA-CL) nanofiber: a biomimetic extracellular matrix for smooth muscle cell and endothelial cell proliferation.* Biomaterials, 2004. **25**(10): p. 1883-90.

66.   Wang, X., B. Ding, and B. Li, *Biomimetic electrospun nanofibrous structures for tissue engineering.* Materials Today, 2013. **16**(6): p. 229-241.

67.   Li, D. and Y. Xia, *Electrospinning of Nanofibers: Reinventing the Wheel?* Advanced Materials, 2004. **16**(14): p. 1151-1170.

68.   Min, B.M., et al., *Electrospinning of silk fibroin nanofibers and its effect on the adhesion and spreading of normal human keratinocytes and fibroblasts in vitro.* Biomaterials, 2004. **25**(7-8): p. 1289-97.

69.   Wang, H., et al., *Synthesis of PDON-b-PEG-b-PDON block copolymers and drug delivery system thereof.* Journal of Applied Polymer Science, 1998. **68**(13): p. 2121-2128.

70.   Rüder, C., et al., *Smooth muscle and endothelial cell behaviour on degradable copolyetheresterurethane films.* Clinical hemorheology and microcirculation, 2012. **52**(2-4): p. 313-323.

71.   Rüder, C., et al., *Viability, proliferation and adhesion of smooth muscle cells and human umbilical vein endothelial cells on electrospun polymer scaffolds.* Clinical Hemorheology and Microcirculation, 2012. **50**: p. 101-112.

72.   Schneider, T., et al., *Viability, Adhesion and Differentiated Phenotype of Articular Chondrocytes on Degradable Polymers and Electro-Spun Structures Thereof.* Macromolecular Symposia, 2011. **309-310**(1): p. 28-39.

73.   Kratz, K., et al., *Shape-Memory Properties and Degradation Behavior of Multifunctional Electro-Spun Scaffolds.* The International Journal of Artificial Organs, 2011. **34**(2): p. 225-230.

74.   Hiebl, B., et al., *Degradation of and angiogenesis around multiblock copolymers containing poly(p-dioxanone)- and poly(ε-caprolactone)-segments subcutaneously implanted in the rat neck.* Clinical Hemorheology and Microcirculation, 2010. **45**: p. 117-122.

75.   Hiebl, B., et al., *In vivo evaluation of the angiogenic effects of the multiblock copolymer PDC using the hen's egg chorioallantoic membrane test.* Clinical Hemorheology and Microcirculation, 2010. **46**: p. 233-238.

76.   Tzoneva, R., et al., *Elastic multiblock copolymers for vascular regeneration: protein adsorption and hemocompatibility.* Clinical hemorheology and microcirculation, 2012. **52**(2-4): p. 337-348.

77.   Jaffe, E.A., et al., *Culture of human endothelial cells derived from umbilical veins. Identification by morphologic and immunologic criteria.* The Journal of clinical investigation, 1973. **52**(11): p. 2745-2756.

78.   Kirkpatrick, C.J., et al., *Physiology and Cell Biology of the Endothelium: A Dynamic Interface for Cell Communication.* International Journal of Microcirculation, 1997. **17**(5): p. 231-240.

79.   DeCicco-Skinner, K.L., et al., *Endothelial cell tube formation assay for the in vitro study of angiogenesis.* J Vis Exp, 2014(91): p. e51312.

80.   Birbrair, A., et al., *Pericytes at the intersection between tissue regeneration and pathology.* Clin Sci (Lond), 2015. **128**(2): p. 81-93.

81.   Risau, W. and I. Flamme, *Vasculogenesis.* Annu Rev Cell Dev Biol, 1995. **11**: p. 73-91.

82.   Tahergorabi, Z. and M. Khazaei, *A review on angiogenesis and its assays.* Iran J Basic Med Sci, 2012. **15**(6): p. 1110-26.

83.   Hauser, S., F. Jung, and J. Pietzsch, *Human Endothelial Cell Models in Biomaterial Research.* Trends Biotechnol, 2017. **35**(3): p. 265-277.

84.   Chamberlain, G., et al., *Concise review: mesenchymal stem cells: their phenotype, differentiation capacity, immunological features, and potential for homing.* Stem Cells, 2007. **25**(11): p. 2739-49.

85.   James, A.W., *Review of Signaling Pathways Governing MSC Osteogenic and Adipogenic Differentiation.* Scientifica, 2013. **2013**: p. 17.

86.   James, A.W., et al., *Perivascular stem cells: a prospectively purified mesenchymal stem cell population for bone tissue engineering.* Stem Cells Transl Med, 2012. **1**(6): p. 510-9.

87.   Mizuno, H., M. Tobita, and A.C. Uysal, *Concise review: Adipose-derived stem cells as a novel tool for future regenerative medicine.* Stem Cells, 2012. **30**(5): p. 804-10.

88.   Levi, B. and M.T. Longaker, *Concise review: adipose-derived stromal cells for skeletal regenerative medicine.* Stem Cells, 2011. **29**(4): p. 576-82.

89.   James, A.W., et al., *Additive effects of sonic hedgehog and Nell-1 signaling in osteogenic versus adipogenic differentiation of human adipose-derived stromal cells.* Stem Cells Dev, 2012. **21**(12): p. 2170-8.

90.   Pei, L. and P. Tontonoz, *Fat's loss is bone's gain.* J Clin Invest, 2004. **113**(6): p. 805-6.

91.   Rutkovskiy, A., K.-O. Stensløkken, and I.J. Vaage, *Osteoblast Differentiation at a Glance.* Medical science monitor basic research, 2016. **22**: p. 95-106.

92.   Kim, B.-S., C.E. Baez, and A. Atala, *Biomaterials for tissue engineering.* World Journal of Urology, 2000. **18**(1): p. 2-9.

93.   Hao, H., et al., *Synthesis and characterization of biodegradable lysine-based waterborne polyurethane for soft tissue engineering applications.* Biomaterials Science, 2016. **4**(11): p. 1682-1690.

94.   Basterretxea, A., et al., *Biocompatibility and hemocompatibility evaluation of polyether urethanes synthesized using DBU organocatalyst.* European Polymer Journal, 2016. **84**: p. 750-758.

95. Mathew, S., et al., *Effect of diisocyanate linkers on the degradation characteristics of copolyester urethanes as potential drug carrier matrices.* European Journal of Pharmaceutics and Biopharmaceutics, 2015. **95**: p. 18-26.

96. Wang, Z., et al., *Effect of Resveratrol on Modulation of Endothelial Cells and Macrophages for Rapid Vascular Regeneration from Electrospun Poly(epsilon-caprolactone) Scaffolds.* ACS Appl Mater Interfaces, 2017. **9**(23): p. 19541-19551.

97. Heydarkhan-Hagvall, S., et al., *Three-dimensional electrospun ECM-based hybrid scaffolds for cardiovascular tissue engineering.* Biomaterials, 2008. **29**(19): p. 2907-14.

98. Jun, I., et al., *Electrospun Fibrous Scaffolds for Tissue Engineering: Viewpoints on Architecture and Fabrication.* Int J Mol Sci, 2018. **19**(3).

99. Wang, X., B. Ding, and B. Li, *Biomimetic electrospun nanofibrous structures for tissue engineering.* Mater Today (Kidlington), 2013. **16**(6): p. 229-241.

100. Neve, A., et al., *Extracellular matrix modulates angiogenesis in physiological and pathological conditions.* Biomed Res Int, 2014. **2014**: p. 756078.

101. Browne, S., et al., *Modulation of inflammation and angiogenesis and changes in ECM GAG-activity via dual delivery of nucleic acids.* Biomaterials, 2015. **69**: p. 133-47.

102. Reid, S.E., et al., *Tumor matrix stiffness promotes metastatic cancer cell interaction with the endothelium.* Embo j, 2017. **36**(16): p. 2373-2389.

103. Black, C.R.M., et al., *Bone Tissue Engineering.* Current molecular biology reports, 2015. **1**(3): p. 132-140.

104. Amini, A.R., C.T. Laurencin, and S.P. Nukavarapu, *Bone tissue engineering: recent advances and challenges.* Critical reviews in biomedical engineering, 2012. **40**(5): p. 363-408.

105. Grablowitz, H. and A. Lendlein, *Synthesis and characterization of α,ω-dihydroxy-telechelic oligo(p-dioxanone).* Journal of Materials Chemistry, 2007. **17**(38): p. 4050-4056.

106. Tung, W.T., et al., *Coaxial electrospinning of PEEU/gelatin to fiber meshes with enhanced mesenchymal stem cell attachment and proliferation.* Clinical Hemorheology and Microcirculation, 2020. **74**: p. 53-66.

107. Rüder, C., et al., *Influence of fibre diameter and orientation of electrospun copolyetheresterurethanes on smooth muscle and endothelial cell behaviour.* Clinical Hemorheology and Microcirculation, 2013. **55**: p. 513-522.

108. Miettinen, M., A. Lindenmayer Ae Fau - Chaubal, and A. Chaubal, *Endothelial cell markers CD31, CD34, and BNH9 antibody to H- and Y-antigens--evaluation of their specificity and sensitivity in the diagnosis of vascular tumors and comparison with von Willebrand factor.* (0893-3952 (Print)).

109. Müller, A.M., et al., *Expression of the endothelial markers PECAM-1, vWf, and CD34 in vivo and in vitro.* (0014-4800 (Print)).

110. LaValley, D.J. and C.A. Reinhart-King, *Matrix stiffening in the formation of blood vessels.* Advances in Regenerative Biology, 2014. **1**(1): p. 25247.

111. Vitorino, P. and T. Meyer, *Modular control of endothelial sheet migration.* Genes Dev, 2008. **22**(23): p. 3268-81.

112. Lo, C.M., et al., *Cell movement is guided by the rigidity of the substrate.* Biophys J, 2000. **79**(1): p. 144-52.

113. Giannone, G., et al., *Periodic lamellipodial contractions correlate with rearward actin waves.* Cell, 2004. **116**(3): p. 431-43.

114. Califano, J.P. and C.A. Reinhart-King, *The effects of substrate elasticity on endothelial cell network formation and traction force generation.* Conf Proc IEEE Eng Med Biol Soc, 2009. **2009**: p. 3343-5.

115. Deroanne, C.F., C.M. Lapiere, and B.V. Nusgens, *In vitro tubulogenesis of endothelial cells by relaxation of the coupling extracellular matrix-cytoskeleton.* Cardiovasc Res, 2001. **49**(3): p. 647-58.

116. DeCicco-Skinner, K.L., et al., *Endothelial cell tube formation assay for the in vitro study of angiogenesis.* Journal of visualized experiments : JoVE, 2014(91): p. e51312-e51312.

117. Trappmann, B., et al., *Extracellular-matrix tethering regulates stem-cell fate.* Nat Mater, 2012. **11**(7): p. 642-9.

118. Olivares-Navarrete, R., et al., *Substrate Stiffness Controls Osteoblastic and Chondrocytic Differentiation of Mesenchymal Stem Cells without Exogenous Stimuli.* PLOS ONE, 2017. **12**(1): p. e0170312.

119. Chancellor, T.J., et al., *Actomyosin tension exerted on the nucleus through nesprin-1 connections influences endothelial cell adhesion, migration, and cyclic strain-induced reorientation.* Biophysical journal, 2010. **99**(1): p. 115-123.

120. Lombardi, M.L., et al., *The interaction between nesprins and sun proteins at the nuclear envelope is critical for force transmission between the nucleus and cytoskeleton.* The Journal of biological chemistry, 2011. **286**(30): p. 26743-26753.

121. Maniotis, A.J., C.S. Chen, and D.E. Ingber, *Demonstration of mechanical connections between integrins, cytoskeletal filaments, and nucleoplasm that stabilize nuclear structure.* Proceedings of the National Academy of Sciences, 1997. **94**(3): p. 849.

122. Bitar, M., et al., *Effect of cell density on osteoblastic differentiation and matrix degradation of biomimetic dense collagen scaffolds.* Biomacromolecules, 2008. **9**(1): p. 129-35.

123. Lu, H., et al., *Effect of cell density on adipogenic differentiation of mesenchymal stem cells.* Biochem Biophys Res Commun, 2009. **381**(3): p. 322-7.

124. McBeath, R., et al., *Cell shape, cytoskeletal tension, and RhoA regulate stem cell lineage commitment.* Dev Cell, 2004. **6**(4): p. 483-95.

125. Canalis, E., *Notch signaling in osteoblasts.* Sci Signal, 2008. **1**(17): p. pe17.

126. Jensen, E.D., R. Gopalakrishnan, and J.J. Westendorf, *Regulation of gene expression in osteoblasts.* Biofactors, 2010. **36**(1): p. 25-32.

127. Sun, M., et al., *Extracellular matrix stiffness controls osteogenic differentiation of mesenchymal stem cells mediated by integrin α5.* Stem cell research & therapy, 2018. **9**(1): p. 52-52.

128. Xu, J., et al., *Potential mechanisms underlying the Runx2 induced osteogenesis of bone marrow mesenchymal stem cells.* American journal of translational research, 2015. **7**(12): p. 2527-2535.

129. Lv, H., et al., *Mechanism of regulation of stem cell differentiation by matrix stiffness.* Stem Cell Research & Therapy, 2015. **6**(1): p. 103.

130. Haase, T., et al., *In vivo biocompatibility study of degradable homo- versus multiblock copolymers and their (micro)structure compared to an established biomaterial.* Clinical Hemorheology and Microcirculation, 2020. **75**: p. 163-176.

131. Santos, M.I. and R.L. Reis, *Vascularization in bone tissue engineering: physiology, current strategies, major hurdles and future challenges.* (1616-5195 (Electronic)).

132. Hofmann, A., et al., *The effect of human osteoblasts on proliferation and neo-vessel formation of human umbilical vein endothelial cells in a long-term 3D co-culture on polyurethane scaffolds.* (1878-5905 (Electronic)).

133. Xu, X., et al., *Controlling major cellular processes of human mesenchymal stem cells using microwell structures.* Adv Healthc Mater, 2014. **3**(12): p. 1991-2003.

Contributions and Acknowledgements

In the following section, the contributions made by other members of the HZG Institute of Biomaterials Science with relation to the work discussed in this thesis are acknowledged.

The multiblock polymers PEEU was provided by Dr. Karl Kratz, Dr. Michael Zierke, and Ms. Monique Hannemann. The molecular weights of the PEEU multiblock copolymers were measured using gas permeation chromatography (GPC) by Dr. Michael Zierke. The electrospinning fiber mesh scaffolds were generated by Mr. Wingtai Tung. The sterilization of the PEEU scaffolds was performed by Dr. Mario Rettschlag. Ms. Susanne Schwanz provided technical support for DSC measurements. Scanning electron microscopy (SEM) experiments were performed by Ms. Yvonne Pieper.

Publications related to this thesis:

Portions of this dissertation have previously been submitted to peer-reviewed journals or have been accepted for publication (see list below). Prof. Dr. Andreas Lendlein and Prof. Dr. Nan Ma designed the research and Prof. Dr. Andreas Lendlein supervised the studies for these publications. All authors were involved in the evaluation of the experimental data and in the composition of the manuscripts, to varying degrees.

1   **Sun X**, Tung W, Wang W, Xu X, Zou J, Gould OEC, Kratz K, Ma N, Lendlein A. The effect of stiffness variation of electrospun fiber meshes of multiblock copolymers on the osteogenic differentiation of human mesenchymal stem cells. Clin Hemorheol Microcirc. 2019;73(1):219-228. doi: 10.3233/CH-199206. PMID: 31561335.

2   **Sun X**, Tung W, Zou J, Wang W, Kratz K, Ma N, Lendlein A. Elasticity of fiber meshes from multiblock copolymers influences endothelial cell behavior. Clin Hemorheol Microcirc. 2020;74(4):405-415. doi: 10.3233/CH-190696. PMID: 31683471.

List of Publications and Conference Abstracts

Publications:

1. **Sun X**, Tung W, Wang W, Xu X, Zou J, Gould OEC, Kratz K, Ma N, Lendlein A. The effect of stiffness variation of electrospun fiber meshes of multiblock copolymers on the osteogenic differentiation of human mesenchymal stem cells. Clin Hemorheol Microcirc. 2019;73(1):219-228. doi: 10.3233/CH-199206. PMID: 31561335.

2. **Sun X**, Tung W, Zou J, Wang W, Kratz K, Ma N, Lendlein A. Elasticity of fiber meshes from multiblock copolymers influences endothelial cell behavior. Clin Hemorheol Microcirc. 2020;74(4):405-415. doi: 10.3233/CH-190696. PMID: 31683471.

3. Tung WT, Zou J, **Sun X**, Wang W, Gould OEC, Kratz K, Ma N, Lendlein A. Coaxial electrospinning of PEEU/gelatin to fiber meshes with enhanced mesenchymal stem cell attachment and proliferation. Clin Hemorheol Microcirc. 2020;74(1):53-66. doi: 10.3233/CH-199235. PMID: 31743992.

4. Li Z, Wang W, Kratz K, Küchler J, Xu X, Zou J, Deng Z, **Sun X**, Gossen M, Ma N, Lendlein A., Influence of surface roughness on neural differentiation of human induced pluripotent stem cells. Clin Hemorheol Microcirc, 2016. 64(3): p. 355-366.

5. Li Z, Xu X, Wang W, Kratz K, **Sun X**, Zou J, Deng Z, Jung F, Gossen M, Ma N, Lendlein A., Modulation of the mesenchymal stem cell migration capacity via preconditioning with topographic microstructure. Clin Hemorheol Microcirc, 2017. 67(3-4): p. 267-278.

6. Zou J, Wang W, Neffe AT, Xu X, Li Z, Deng Z, **Sun X**, Ma N, Lendlein A., Adipogenic differentiation of human adipose derived mesenchymal stem cells in 3D architectured gelatin based hydrogels (ArcGel). Clin Hemorheol Microcirc, 2017. 67 (3-4): p. 297-307.

Conference Abstracts:

1. 38th Annual Meeting of the German Society for Clinical Microcirculation and Hemorheology, 21–23 November 2019, Braunschweig, Germany. (Abstract & short presentation).
   Title: The Effect of stiffness variation of electrospun fiber meshes of multiblock copolymers on the osteogenic differentiation of ADSC

2. Polydays 2019–Polymer Science and Engineering in View of Digitalization, 11–13 September 2019, Berlin, Germany. (Abstract & Poster).

Title: Elasticity of fiber meshes from multiblock copolymers influences endothelial cell behaviors

3. Advanced Functional Polymers for Medicine 2019, 5–7 June 2019, Espoo, Finland. (Abstract & Poster).

   Title: Elasticity of fiber meshes from multiblock copolymers influences endothelial cell behaviors

4. MacroBio Summer School. June 2017. A lecture on Cell-Material interactions-Biocompatibility of Materials, Germany.

Curriculum Vitae

Personal Details

Name: Xianlei Sun

Nationality: People's Republic of China (PRC)

Email: sunxianlei88@gmail.com

Educational Background

10/2015-Present: Ph.D candidate, Helmholtz Macrobio Graduate School, Teltow and Potsdam Universität.

09/2012 -07/2015: Master's degree of Radiology Medicine, Basic Medical School, Peking University (PRC).

09/2007-07/2011: Bachelor's degree of Biotechnology, Shandong University (PRC).

Language:

1. English: Fluent in reading and scientific writing, good in speaking.

2. Mandarin: Mother tongue.